THESIS FOR THE DEGREE OF DOCTOR OF PHILOSOPHY

Iron-nitrogen containing carbon catalysts for oxygen reduction in fuel cells

Synthesis, structural characterization and electrochemical evaluation

CAROLINE JANSON

Department of Chemistry and Chemical Engineering
CHALMERS UNIVERSITY OF TECHNOLOGY
Göteborg, Sweden 2018

Iron-nitrogen containing carbon catalysts for oxygen reduction in fuel cells
Synthesis, structural characterization and electrochemical evaluation

CAROLINE JANSON
ISBN 978-91-7597-736-2

Doktorsavhandlingar vid Chalmers Tekniska Högskola
Ny serie nr 4417
ISSN 0346-718X

Department of Chemistry and Chemical Engineering
Chalmers University of Technology
SE-412 96 Gothenburg
Sweden
Telephone + 46 (0)31-772 1000

Cover: Schematic illustration of a single cell proton exchange membrane fuel cell (left), an iron-chelating ordered mesoporous carbon catalyst (middle), and an electron paramagnetic resonance spectrometer (right).

Printed by:
Chalmers Reproservice
Gothenburg, Sweden 2018

Iron-nitrogen containing carbon catalysts for oxygen reduction in fuel cells
Synthesis, structural characterization and electrochemical evaluation

CAROLINE JANSON

Department of Chemistry and Chemical Engineering
CHALMERS UNIVERSITY OF TECHNOLOGY

ABSTRACT

New solutions to efficiently convert energy are needed to mitigate global climate changes and sustain the needs of the growing population. An energy device with high potential is the proton exchange membrane (PEM) fuel cell. PEM fuel cells can convert chemical energy to electrical energy with extraordinary high conversion efficiency. However, a drawback with PEM fuel cells is their high price, mainly caused by extensive use of the expensive noble metal platinum as catalyst in the fuel cell cathode. A reduced catalyst price (ideally by replacing platinum) would make PEM fuel cells' cost-competitive in comparison to other energy conversion devices. Consequently, the development of inexpensive noble metal-free catalysts, active for the oxygen reduction reaction (ORR) has become a hot research topic.

In this thesis, we designed and synthesized iron-chelating nitrogen-functionalized ordered mesoporous carbon (Fe-OMC) catalysts, active for ORR in PEM fuel cells. One focus of the work was to gain a deeper understanding about the operational mechanism of the active sites in the catalysts. Another focus was to evaluate the influence of some synthesis variables and gain new insight into the formation mechanism of the materials to thereby achieve more active catalysts. Several steps are covered in the thesis; synthesis of Fe-OMCs, physical characterization of the catalysts, structural investigation of the active sites, and electrochemical evaluation of the catalysts in a single cell PEM fuel cell. Characterization methods, such as N_2-sorption, Raman, X-ray diffraction, and Small Angle X-ray scattering, were used to investigate the physical properties of the catalysts. Whereas, electron paramagnetic resonance (EPR) and nuclear magnetic resonance (NMR) spectroscopies were used to study the active sites and iron-nitrogen interactions in both the precursor mixtures and the final catalysts. In this thesis EPR spectroscopy was (for the first time) shown to be a useful method to study Fe-OMC (and possibly other Fe-N/C) catalysts. It was shown that EPR spectroscopy can contribute with substantial information regarding the iron species, oxygen radicals, and delocalized electrons in the Fe-OMCs. Essential information about the iron species such as type, oxidation state, geometry and interaction with oxygen was obtained. Of more general importance, a number of crucial pretreatment steps of the EPR samples were identified and found necessary to employ prior to the measurements to obtain high quality EPR data.

Furthermore, additional information about the Fe-N_x chelate structures acting as catalytically active sites was successfully obtained by comparing catalysts prepared from precursors with different functional groups. The results confirmed that nitrogen is involved in the formation of active sites in the Fe-OMC catalysts. Iron-nitrogen interactions could be observed in the precursor mixing step of the catalyst preparation and were correlated to catalytic activities in the final catalysts. Synthesis parameters such as hydration state of the iron salt, precursor aging time, iron to N/C-precursor ratio, iron salt anion, were shown to influence the performance of the prepared catalysts. Finally, by modifying the precursor composition and employing an alternative template etch method, improvements of the mesoporous carbon properties were achieved.

With the results obtained, we made progress in the understanding and tuning of Fe-OMC catalysts. Even though the catalytic performance of these new noble metal-free catalysts is still inferior the commercial platinum-based catalysts, they seem to have potential to compete with them and hopefully, eventually replace them in applications for PEM fuel cells.

Keywords: *fuel cell, oxygen reduction reaction, mesoporous carbon, cathode catalyst, non-precious metal catalyst, active site, electron paramagnetic resonance.*

List of Publications

I. Influence of Iron Precursor Hydration State on Performance of Non-Precious Metal Fuel Cell Catalysts

C. Janson, J. K. Dombrovskis and A. E. C. Palmqvist

*Published in Journal of Materials Chemistry A, 2018, **6**, 3116-2125*

II. Influence of Precursor Functional Groups on the Formation and Performance of Iron-Coordinating Ordered Mesoporous Carbons as Fuel Cell Catalysts

C. Janson and A. E. C. Palmqvist

*Published in Journal of Physical Chemistry C, 2017, **121**, 21827-21835*

III. Improved Oxygen Reduction Activity of Transition Metal-Chelating Ordered Mesoporous Carbon Fuel Cell Catalysts by Milder Route of Preparation

C. Janson and A. E. C. Palmqvist

Manuscript

IV. Influence of Iron Salt Anions on Formation and Oxygen Reduction Activity of Fe/N-Functionalized Mesoporous Carbon Catalysts

S. J. Fretz, C. Janson, W. R. Arbelaez and A. E. C. Palmqvist

Manuscript

V. Electron Paramagnetic Resonance Spectroscopy Analysis of Iron-Chelating Ordered Mesoporous Carbons for Oxygen Reduction Fuel Cell Catalysts

C. Janson and A. E. C. Palmqvist

Manuscript

Contribution Report to the listed Publications

I. Responsible for the synthesis and data analysis of the samples prepared for the NMR, RDE, and TEM measurements, the discussion regarding the NMR, RDE, and TEM measurements, the catalysts prepared from the NMR samples and fuel cell testing of these. Responsible for restructuring and clarification of the manuscript and writing the current version of the manuscript.

II. Responsible for all experimental work, with assistance to set up EPR, NMR, and Raman measurements. Responsible for all data analysis, writing the first draft and the major part of the manuscript.

III. Responsible for all experimental work. Responsible for all data analysis, writing the first draft and the major part of the manuscript.

IV. Responsible for the fuel cell testing and the EPR experiments and the data analysis of fuel cell and EPR results. Responsible for the discussion regarding the fuel cell and EPR measurements as well as contributing with comments regarding the whole manuscript.

V. Responsible for all experimental work. Responsible for all data analysis, writing the first draft and the major part of the manuscript.

TABLE OF CONTENTS

Till en okänd efterkommande

Jag bröt mitt bröd, som andras hand fått baka,
och drack mitt vin, som jag ej själv beredde.
De, som haft mödan, fingo aldrig smaka
dess frukt, förrn de på mörka vägar trädde.

Vad jag har sått, skall du i morgon skörda.
O må mitt säde hundrafaldigt bära!
De bära fröjd, som bära andras börda,
de skära liv, som andras skördar skära.

Karin Boye, ur diktsamlingen *Moln*

1. Motivation

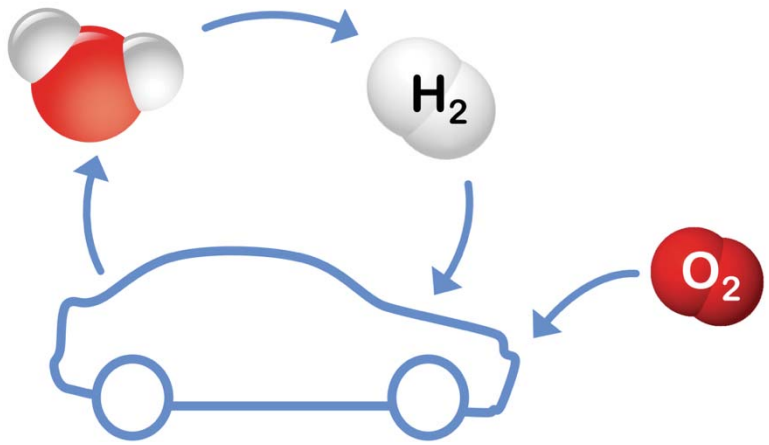

To change the course of our society, sustainable development is needed. As an effect of the industrial revolution, the increasing population, and people's desire for economic improvement we now experience complications. The rising global energy consumption, the dependence on diminishing fossil fuel resources and the greenhouse effect could be seen as some of the most challenging ones.[1-2] We basically need new solutions to produce more energy in forms that are useful for us, by efficiently converting energy from one form to another.

In the long term, we need to develop energy conversion devices based on fully renewable energy sources such as solar, wind and water energy, which do not pollute or contribute to the global warming. Downsides with these renewable energy sources are their unpredictability and variation in energy supply. In many applications, continuous and controllable energy supply is necessary. Batteries and other energy storage solutions can compensate for these fluctuating behaviours to some extent, although these energy devices then become more complex and dependent on both the renewable energy source and the storage solution. A more immediate solution would be to use fossil fuels more efficiently and find ways to utilize alternative sources of carbon from plants. The CO_2 emissions would then remain, but be reduced.

A technology which could contribute to both a long term and immediate solution is the *fuel cell technology*. In a fuel cell, chemical energy (in the fuel) is efficiently converted to electrical energy via chemical reactions. Fuel cells can be used in both stationary and mobile applications with a controlled energy supply and high reliability. The most common fuel cell type today is the proton exchange membrane (PEM) fuel cell. The PEM fuel cell is fueled by hydrogen and oxygen and the only exhaust-product formed is water. Oxygen is easily accessible and the oxygen fraction in the air is enough to fuel the cell. The hydrogen production is more complicated and today most hydrogen is produced from steam reforming of hydrocarbons (fossil fuels). Production of hydrogen via electrolysis of water is a more sustainable alternative, but so far, only small quantities are produced globally since the process is relatively energy consuming and expensive.[3] Encouragingly, the water-splitting research today is an attractive field[4] and the solutions, for example photocatalysis,[5] are continuously improved. With sustainable hydrogen production available, the fuel cell technology has potential to be one of the most sustainable energy converting solutions of our time. By combining solar or wind-powdered water electrolysis, hydrogen storage, and fuel cell technology, there are great potentials to develop efficient, reliable and green energy conversion devices necessary for the future.

But why should it be simple? As it will be described in this thesis, improvements in the fuel cell technology itself are fundamental and perhaps the most crucial for the commercialization and market development of fuel cell technology. One of the main problems is the catalysts, since PEM fuel cells need relatively large amounts of catalysts to work efficiently. The most efficient and commonly used catalysts today for both the anode and the cathode in PEM fuel cells are based on platinum. Platinum is not only a rare and noble metal, due to its extraordinary physical and chemical properties, platinum is precious and sometimes irreplaceable in certain industrial applications.[6] Consequently, platinum is a very expensive metal and accordingly this makes the price of PEM fuel cells comparably high.[7] The current use of platinum catalysts, is one of the main reasons for the slow commercial development and limited market introduction of PEM fuel cells. In order to make these fuel cells economically competitive to other energy conversion devices the cost of the catalyst has to be reduced. Therefore, it is of interest to develop new, inexpensive noble metal-free catalysts with similar properties in terms of catalyst conversion efficiency and operation stability as the platinum-based catalysts.[8] And that is what this thesis work is about.

1.1 Objective

This project aims to design and synthesize materials with the purpose to find a simple, inexpensive way to prepare efficient noble metal-free catalysts active for the oxygen reduction reaction. An already developed method to produce such catalysts is used as a starting point.[9-11] The focus in this thesis is to tune and simplify this method to produce iron-chelating ordered mesoporous carbon (Fe-OMC) catalysts with improved catalytic activity. Also emphasized in this thesis, is to develop a deeper understanding of the operational mechanism behind the active site in the catalysts, and explore analytical methods to study it.

Practically, the thesis process covers several steps. The first step *(i)* is synthesis of Fe-OMCs followed by *(ii)* physical characterization of the material properties of catalysts and *(iii)* structural investigation of the active sites. Subsequently, the catalyst is *(iv)* electrochemically evaluated in a single cell PEM fuel cell. Thereafter, *(v)* correlations between results are made and modifications in the synthesis proposed. The synthesis is repeated with proposed adjustments and the loop *(i-v)* continuous in order to tune the synthesis and reach a more and more active, efficient and cheap catalyst.

To be noted is that the investigations of the active sites in the catalysts are done by less employed methods in the field such as electron paramagnetic resonance and paramagnetic nuclear magnetic resonance spectroscopies. We believe we can gain new knowledge with these methods and eventually, we hope to contribute with information that can make synthesis of noble metal-free catalysts more efficient and generate highly active and sustainable catalysts.

2. Fuel Cells – Theory and Performance

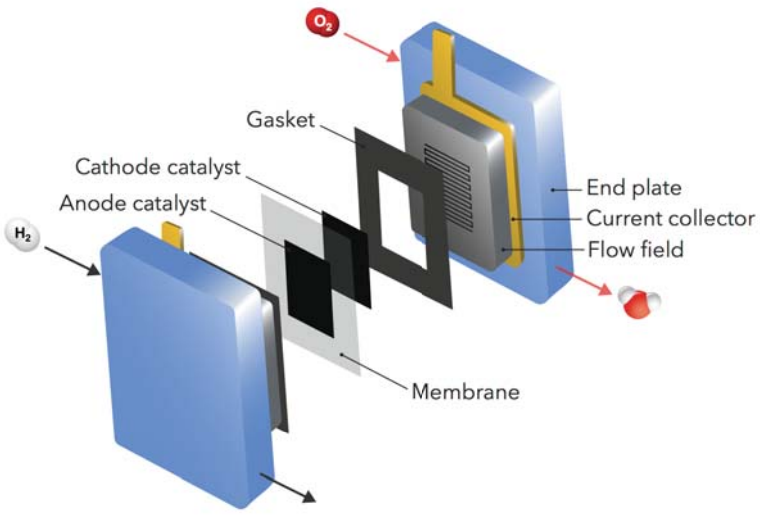

2.1 Historical review

A fuel cell is an electrochemical cell which can convert chemical energy in fuels directly into electrical energy through chemical reactions. Distinct from a battery, the reactants for the two electrode reactions in a fuel cell are stored externally outside the cell. As a consequence, the energy output from a fuel cell system depends on both the cell performance (how efficient the chemical energy is converted to electrical energy) but also the dimensions of the fuel storage tanks and the possibility to refill or replace them.

The fuel cell concept was demonstrated already in 1801 by Humphry Davy,[12] and 1839 William Grove[13] invented the first working fuel cell. After that, improvements in the fuel cell technology were slow and it was not until the first space exploration programs fuel cells gained enough interest for development and applications because of its ability to produce both energy and water. In 1966 the first fuel cell vehicle (*GM Electrovan*)[14] was built, but the project was later cancelled because of high cost. Since then and especially in the last two decades, fuel cells have been "up-and-coming" in the automobile industry although the progress has been slower than expected. Today, most car companies have designed a prototype fuel cell car for potential replacement of the combustion engine cars. Toyota, Hyundai, and Honda, are in the fore front and they lately released fuel cell cars for retail sales and lease contracts in the US, Europe and Japan.[15] The prices of these cars are still high compared to regular cars but they are decreasing rapidly. Fuel cells are being developed for other transportation vehicles as well, such as buses, trains, airplanes, boats and forklifts. Besides the automotive industry fuel cells are also used for many other applications such as stationary power plants, combined heat and power stations, and emergency power supplies. Fuel cells, in combination with electrolysers, can also be used for large scale energy storage necessary in connection with solar and wind energy production.[16]

Several types of fuel cells exist, commonly classified by their electrolyte.[16-17] They are working in different temperature and pH-conditions and with various types of fuels and are therefore suitable for different types of applications as shown in Figure 1. The most common fuel cells are the proton exchange membrane fuel cell (PEMFC), the alkaline fuel cell (AFC), the phosphoric acid fuel cell (PAFC) (all three working at relatively low temperatures), the solid oxide fuel cell (SOFC) and the molten carbonate fuel cell (MCFC) (working at high temperatures). The main disadvantages

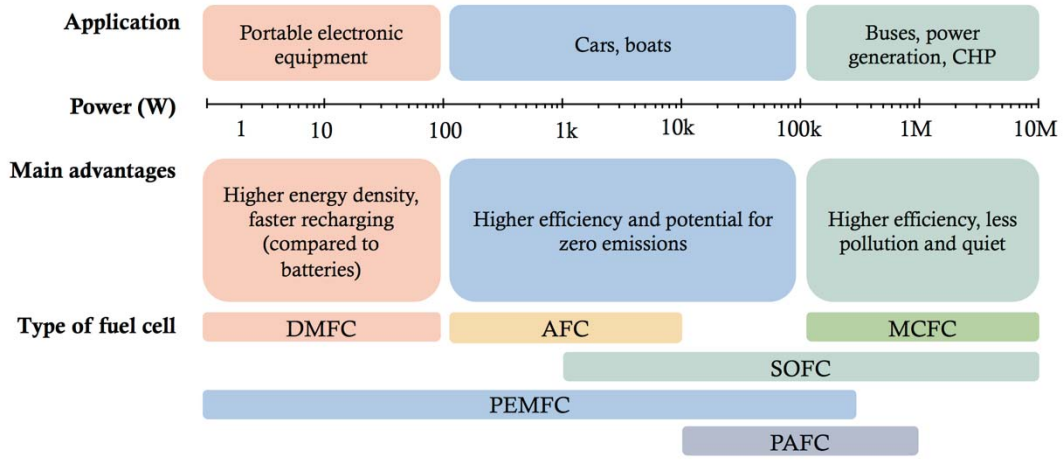

Figure 1. Summary of applications and advantages for different kinds of fuel cells. Modified from reference.[16]

with fuel cells nowadays is their price, and a lot of research, is focused on reducing cost. However, advantages with using fuel cells are their high efficiency and relative simplicity. Fuel cells are generally more efficient than piston and turbine based combustion engines and also simpler because of their few moving parts, making them silent, reliable and long-lasting systems. Furthermore, in most fuel cells the only by-product is warm water, meaning zero emissions during operation. However, it should be noted that during the production of hydrogen, in most cases, emissions of CO_2 occur.

2.2 Proton Exchange Membrane Fuel Cells

Proton exchange membrane fuel cells or polymer electrolyte membrane fuel cells (PEMFCs) are the most commonly used fuel cell type and in focus in this thesis. In later sections, when discussing subjects regarding the principle and performance of fuel cells it will basically only concern PEMFCs. The PEMFC is usually fueled with hydrogen and oxygen (air), but other fuels like methanol in a direct methanol fuel cell (DMFC), ethanol in a direct ethanol fuel cell (DEFC), and dimethyl ether in a direct dimethyl ether fuel cell (DDMEFC) are also used. The only exhaust-product formed from the hydrogen fueled PEMFC is water.

One single cell in the PEMFC consists of several layers, as shown in Figure 2. The outer layers consist of bipolar plates followed by gas diffusion layers, with the purpose to collect and transfer the produced current and also distribute the gas flow uniformly over the catalyst. The middle part is the heart of the PEMFC containing two catalyst layers separated by a thin humidified proton conductive polymer membrane. These three layers are usually referred to as the membrane electrode assembly (MEA). The proton conductive polymer frequently used in PEMFCs is a perfluorinated sulfonic acid polymer called Nafion® and the most commonly used catalysts, for both the anode and the cathode, are platinum nanoparticles dispersed on a carbon support. [17]

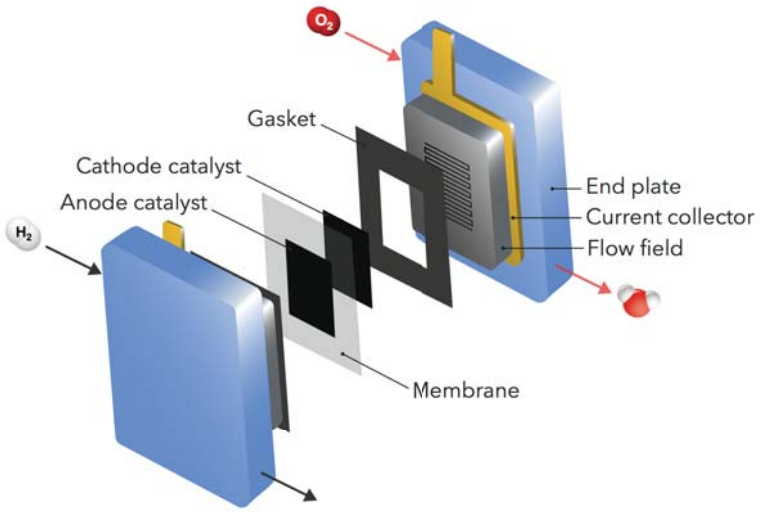

Figure 2. Schematic illustration of a single cell PEMFC.

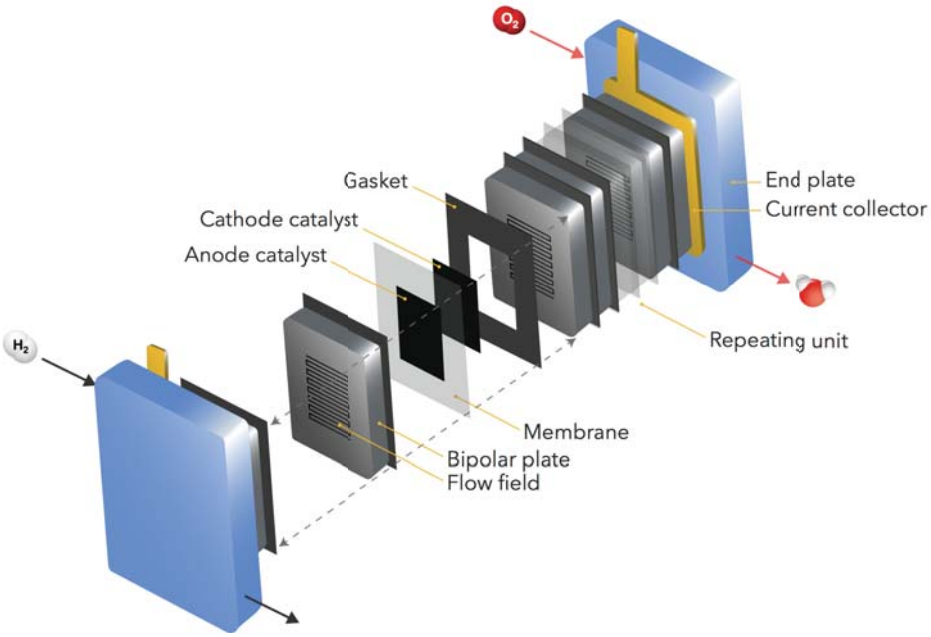

Figure 3. Schematic illustration of a PEMFC-stack.

Multiple of these cells can be connected in series (shown in Figure 3), in a stack, to increase the power output. In this thesis, we concentrate on understanding the cathode and its catalytically active sites. To avoid unwanted parameters influencing the performance, which may occur when using a fuel cell stack, a simple single cell PEMFC setup was used in all experiments. An advantage with PEMFCs is the thickness of the MEAs which creates opportunities to produce highly compact fuel cell stacks with high power density. Additionally, the absence of corrosive fluids in PEMFCs makes them user-friendly and possible to orient in any direction and therefore suitable for applications such as vehicles and portable electronic equipment.

The PEMFC's operation temperature typically ranges between 20°C and 80°C and is limited by the proton exchange membrane which loses its function at too high temperatures. An advantage with such low working temperature is short start up time to reach optimal performance. However, a drawback with low working temperature is that the use of catalysts becomes extra demanding, since the fuel cell reactions occur slower at low temperature.

2.3 Hydrogen production and storage

Important issues which have to be highlighted regarding PEMFCs are the production and storage of hydrogen. As mentioned above PEMFCs are fueled with hydrogen and oxygen. The oxygen fraction in the air is enough to fuel the cell. However, the hydrogen is mainly produced by steam reforming or partial oxidation of fossil methane, natural gas, oil or coal. In the production, considerable amounts of CO_2 (9-12 ton per ton produced hydrogen)[18-19] are created, so claiming PEMFCs today to be "green" and renewable-energy-based is incorrect. Another way to produce hydrogen is by splitting water via electrolysis. Electrolysis has a great potential especially in combination with energy conversion devices based on fully renewable energy sources (solar, wind

and water).[4] Hydrogen produced via electrolysis could, in theory, result in zero greenhouse gas emissions. The electrolysis production of hydrogen allows for storage of "renewable energy". In times of excess energy (a windy or sunny day), the converted excess electricity can be used to produce hydrogen, which can be used as a fuel when needed (for example in a fuel cell car).

The other difficulty with hydrogen gas usage is the storage. Techniques used today, such as high pressure and cryogenics, require lots of energy to maintain. However, the field has been undergoing considerable developments the last decades and solutions are coming, especially in the research for usage of hydrogen in lightweight and compact energy applications such as the automobile industry. An example of a promising and safe solution is carbon-composite technology for high pressure tanks (up to 700 bar).[20]

2.4 PEMFC Working Principle

In a fuel cell, the output electrical energy is gained from the chemical energy "stored" in the fuel. The overall reaction in a PEMFC is spontaneous, i.e. the Gibbs free energy of the reaction is negative.[16] This means that the energy level of the reactants (oxygen and hydrogen) are higher than the energy of the product (water). If mixing hydrogen with oxygen directly a highly exothermic reaction would occur producing heat and water, see Reaction Scheme 2.1. The reaction has a high activation barrier, however, and requires a catalyst to reach high reaction rates.

$$2H_2 + O_2 \rightarrow 2H_2O + heat \qquad [2.1]$$

$$2H_2 \rightarrow 4H^+ + 4e^- \qquad [2.2]$$

$$O_2 + 4H^+ + 4e^- \rightarrow 2H_2O \qquad [2.3]$$

In a fuel cell, the energy from the chemical reaction can be released in a controlled way and electrical energy can be produced by separating the reaction into two cell reactions. In an acid electrolyte fuel cell as a PEMFC, see Figure 4, hydrogen is split into protons and electrons at the anode as in Reaction Scheme 2.2. This reaction is often referred to as the hydrogen oxidation

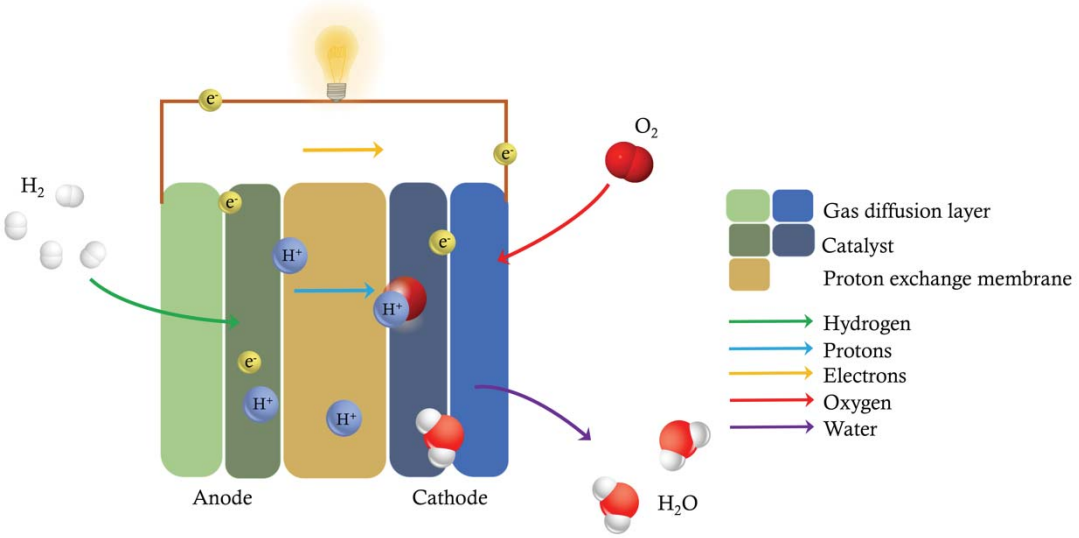

Figure 4. Schematic illustration of the basic principles of a PEMFC.

reaction (HOR). In parallel, the protons are transported through the proton exchange membrane whereas the electrons are forced through an external circuit in a current that can be used to drive an electric device. At the cathode, the protons and the electrons recombine, and together with oxygen they form water as in Reaction Scheme 2.3. This reaction is often referred to as the oxygen reduction reaction (ORR). Both reactions happen simultaneously and are dependent on each other in order to proceed. The rate of the reactions is dictated by the power required from the electric device. This means that at low power needs the reactions will occur with reaction rates required to reach the power need. At higher power needs, the power outcome is limited by the maximum reaction rates achievable by the fuel cell.

2.5 The need for catalysts and high electrode surface areas in PEMFCs

Despite the fact that Gibbs free energy of the overall fuel cell reaction is negative, the overall fuel cell reaction behaves unspontaneous and slow. For a reaction to happen the energy in the system has to overcome the activation energy illustrated by the red line in Figure 5a. To overcome the slow reaction rates, methods such as use of *(i)* catalysts, *(ii)* increased reaction temperature, and/or *(iii)* increased electrode surface area can be applied.[16] In PEMFCs the proton exchange membrane Nafion® is commonly used. Nafion® gradually loses its proton transfer functions at higher temperatures than 80°C so the temperature becomes a limiting factor. Therefore, in low temperature fuel cells such as PEMFCs, the use of catalysts and high electrode area are of extra importance. A catalyst lowers the activation energy of a reaction (illustrated by the green line in Figure 5a), resulting in an increased reaction rate. Both the HOR and the ORR are relatively slow reactions, so catalysts are required on both the anode and the cathode side. The most efficient and commonly used catalysts today for both the HOR and ORR are based on platinum. For the HOR relatively small amounts of platinum is necessary to achieve high efficiency. However, for the ORR, considerable amounts of platinum catalyst are needed to reach a decent efficiency which makes the ORR the rate limiting reaction and by far the largest source of loss in efficiency in the PEM fuel cell.

In a catalyst, it is at the *active site* the reaction takes place. In the ORR, electrons (usually coming from a conductive solid phase), protons (in liquid phase) and oxygen (in gas phase) meet and react in a triple phase boundary[16] and the active site assists with this boundary as shown in Figure 5b. Clearly, a high electrode surface electrode area is of advantage. If the electrode area is large, more active sites can fit per unit mass of catalyst, and a higher reaction rate can be achieved. Usually this is done by using a catalyst support with large specific surface area.

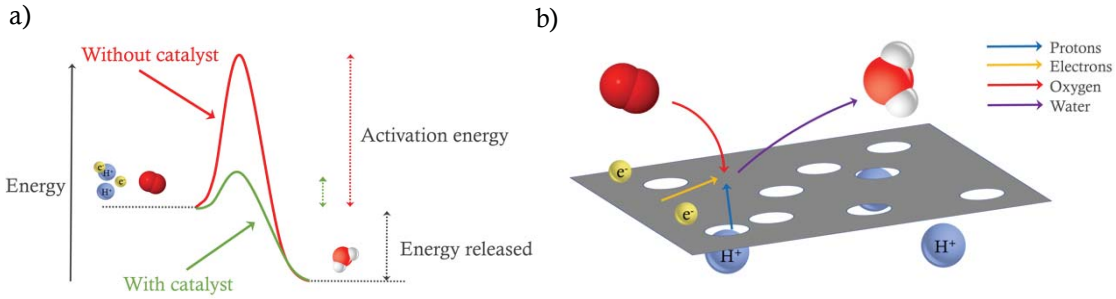

Figure 5. Schematic illustrations of (a) an energy diagram of the ORR with (green) and without (red) catalyst and (b) a triple phase boundary catalyst electrode where oxygen, protons, and electrons meet and form water.

2.6 Fuel Cell Efficiency

In a fuel cell the output electrical energy is gained from the chemical energy "stored" in the fuel.[21] The Gibbs free energy of formation ($\Delta\bar{G}_f°$) of water, (as in Reaction Scheme 2.1) always has a negative value (although it varies with temperature) meaning energy is released. In a reversible case (zero energy losses in the fuel cell), all the chemical energy would be converted into electrical energy. The electrical work done moving the charge around the system is:

$$\textit{electrical work done} = \textit{charge x voltage} = -2FE \qquad [2.4]$$

Where F is the *Faraday constant* ($F = N_A e = 96485\ C$) describing the charge of one mole of electrons, and the *2* comes from two electrons produced per mole hydrogen.[21] In a reversible case the electrical work done is equal to the Gibbs free energy released (*electrical work done* = $\Delta\bar{G}_f°$). The reversible open circuit voltage or the electromotive force (EMF) can then be calculated from:

$$E_{reversible} = \frac{-\Delta\bar{G}_f°}{2F} \qquad [2.5]$$

Since fuel cells are converting chemical energy of fuels that are usually burnt, the efficiency of the fuel cells is commonly defined comparing the electrical energy produced with the corresponding heat which would be produced by burning the same fuel:

$$\eta_{reversible} = \frac{\Delta\bar{G}_f°}{\Delta\bar{H}_f°} \qquad [2.6]$$

The highest theoretical open circuit voltage and efficiency that could be reached in a PEM fuel cell at 25°C and standard conditions are 1.23 V and 83 % forming liquid water. In Figure 6, the theoretical efficiency at different operating temperatures are compared to the maximum theoretical efficiency of a heat engine (Carnot cycle).[21] The graph shows that the theoretical maximum fuel cell efficiency decreases with increasing temperature. The graph also shows that

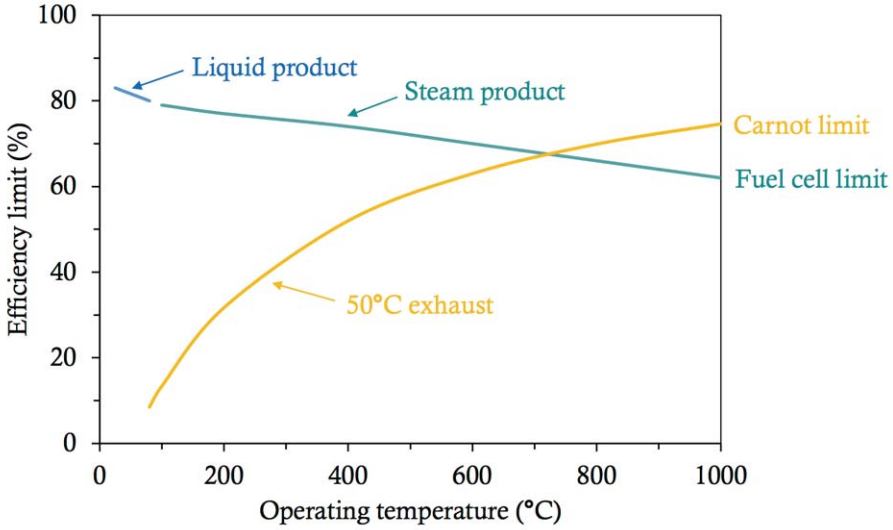

Figure 6. Highest theoretical hydrogen fuel cell efficiency varying with temperature compared to the highest theoretical efficiency of a heat engine. Reproduced from reference.[21]

the fuel cell efficiency is higher than the efficiency of a heat engine to a certain temperature. To be noted is that the theoretical image of the efficiency looks quite different from the practical image since losses occur in both the fuel cell and in heat (combustion) engines.[22] To calculate the real efficiency of the fuel cell one has to consider losses in the fuel cell. While running the cell the actual cell voltage V_{cell} can be obtained (which will be lower than the theoretical value) in which the cell losses are included. The real fuel cell efficiency can then be calculated as follows:

$$\eta_{cell} = \frac{V_{cell}}{E_{reversible}/\eta_{reversible}} \qquad [2.7]$$

2.7 Electrochemistry of PEMFCs

The power output of the fuel cell is of interest to be able to compare it to other electric power generators. Fuel cells and fuel cell stacks are often designed for specific purposes, where the power output required for certain application can vary from milliwatt to megawatt. The power for a cell can be defined as:

$$Power = IV_{cell} \qquad [2.8]$$

Where the unit is given in watts (W) (and in this context W is usually given per unit area of electrode). The fuel cell performance is therefore commonly presented in terms of *cell potential* (in voltage) and *current densities* (in ampere/cm^2) in a polarization curve as shown in Figure 6. To be able to compare fuel cells to other electric power generators, certain key values/graphs are used for comparison. One such value is the current density (current per unit area) at a given voltage (usually 0.6 or 0.7 volt) with the unit $mAcm^{-2}$. From that value the power per unit area can be calculated with the unit $mWcm^{-2}$.[23]

2.8 Performance losses in fuel cells

The fuel cell never performs ideally. Inefficiencies in the cell cause losses which are described as the *overpotential*.[24] The overpotential is the difference between the theoretical cell potential and the experimentally observed cell potential as shown in Figure 7. In a fuel cell context, it means that less output electrical energy is obtained than what is thermodynamically expected. The cell potential (V_{cell}) reflects how efficiently the fuel cell converts chemical energy to electrical energy:

$$V_{cell} = E_{reversible} - \eta_a - \eta_c - IR \qquad [2.9]$$

W here $E_{reversible}$ is the reversible potential of the anode and the cathode reaction, η_a and η_c are the overpotentials caused by the anode and cathode and the IR is a voltage drop caused by resistance inefficiencies.[23] The overpotential (polarization) caused by the cathode is by far the largest inefficiency in the fuel cell as illustrated in Figure 8. The overpotential is explained by energy losses in the fuel cell generating heat. There are four main types of losses in PEMFC and they are described below.

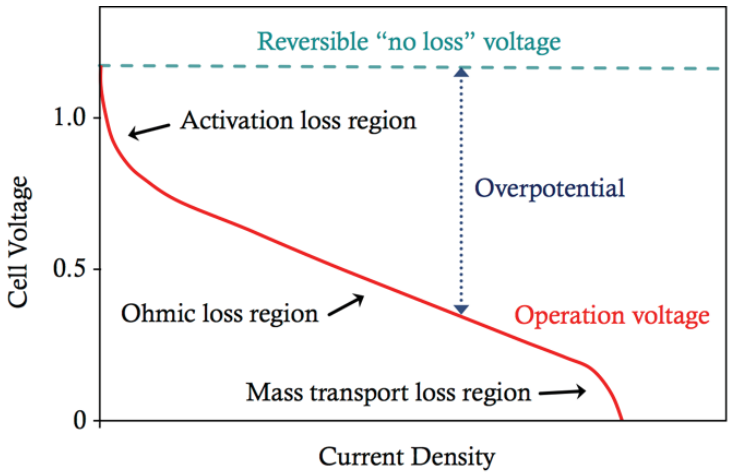

Figure 7. Schematic illustration of energy losses in PEMFCs. Reproduced from reference.[24]

2.8.1 Activation losses

Perhaps the most important irreversible loss in the PEM fuel cells is the activation overpotential and can be correlated to the voltage drop at low currents in the polarization curve (see Figures 7 and 8). The activation loss is caused by lack of activity of the catalyst making the reactions slow, in particular at the cathode side for oxygen reduction reaction which is the slowest and limiting reaction (Equation 2.3).[21] At open circuit voltage (OCV) or zero current density one may think that there is no activity on the cathode. However, the ORR occurs all the time but so does also the reverse reaction with the same rate, forming an equilibrium:

$$O_2 + 4H^+ + 4e^- \leftrightarrow 2H_2O \qquad [2.10]$$

These reactions will cause a flow of electrons back and forth through the cell and can be referred to as the *exchange current density* (i_0). The more active the catalyst is, the more electrons can flow back and forth and cause a larger exchange current density. The higher the exchange current density, the lower the activation overpotential. For simple systems, the exchange current density can be calculated using a *Tafel plot*. There is no catalyst which is ideal and can perform the back-and-forth reaction to 100%, resulting in a lower experimental OCV compared to the theoretical OCV. However, to reduce the activation overvoltage one can try to increase the exchange current density. This can be done by raising the temperature (high temperature fuel cells have much less activation overpotential), increase the activity of the catalyst, increase the catalyst surface area, increase the reactant concentration and/or increase the oxygen partial pressure. These are properties which should be considered when designing a catalyst.

2.8.2 Fuel crossover and internal currents

In PEM fuel cells, it is very likely that small amounts of hydrogen migrate through the proton exchange membrane and end up reacting on the cathode without producing any current. Electrons can also pass, in a similar way, from the anode to the cathode internally without producing any

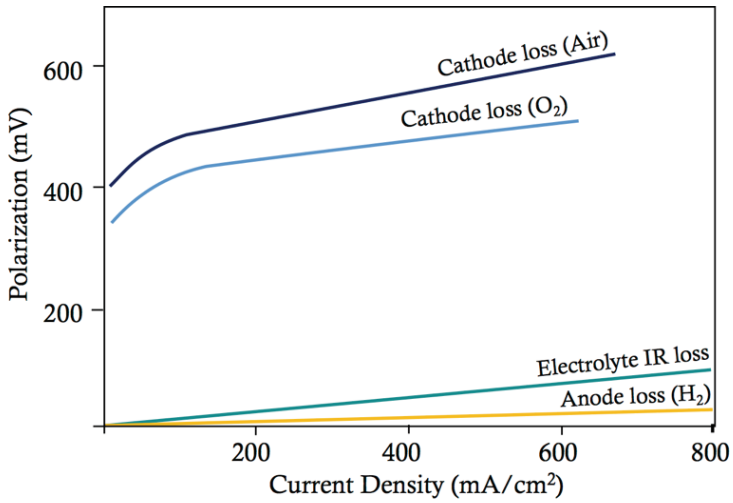

Figure 8. Contribution to energy losses in PEMFCs. Reproduced from reference.[17]

current. These phenomena are known as fuel crossover and internal currents.[21] They especially have an effect on the OCV in PEM fuel cells and can lower the voltage with about 0.2V compared to the theoretical value and they also make the OCV highly variable. Unfortunately, the fuel crossover and internal currents are difficult to measure.

2.8.3 Ohmic losses

The linear part in the polarization-curve (see Figure 7) corresponds to electrical resistance in and in between the electrodes, contacts, etc., and resistance in the flow of ions in the electrolyte, resulting in an ohmic loss (or IR-drop).[21] To reduce the internal resistance in the cell it is important to use conductive materials, proper interconnects between different components in the cell, and making the MEA optimally thin.

2.8.4 Mass transport losses

At higher currents (see Figure 7) the losses mainly correspond to mass transport and/or concentration losses in the fuel cell. This can be caused by a concentration reduction of hydrogen (at the anode) or oxygen (at the cathode) dependent on the consumption rate of the reactants. Furthermore, the water formed during the reaction may block the active site and/or the transportation of oxygen gas. Factors which influence the mass transport/concentration losses are the circulating options for the gases, the flowrate and the partial pressure of the gases, and the activity of the catalysts.[21]

3. Non-precious Cathode Catalysts for Oxygen Reduction

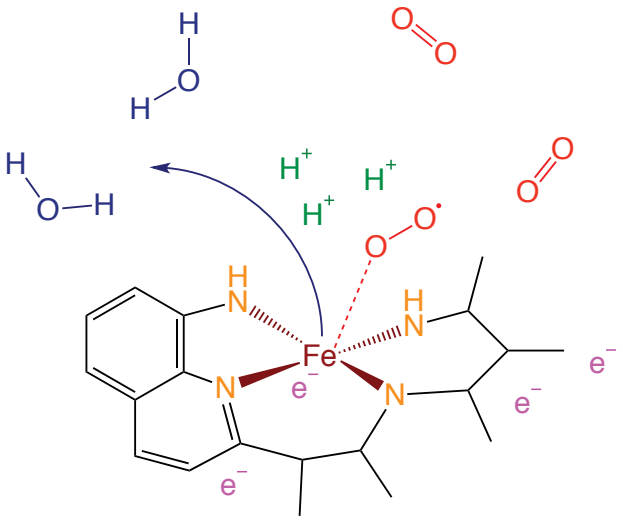

3.1 The need for non-precious catalysts

As discussed in Section 2.5, PEMFCs require considerable amounts of platinum catalysts on the cathode side to work efficiently. The noble metal platinum is one of few materials which is stable to corrosion and dissolution in the acidic environment at the ORR potential. Moreover, platinum is a precious and rare metal and due to its extraordinary physical and chemical properties it is sometimes irreplaceable in certain industrial applications. This makes platinum very expensive, and as a consequence the price of PEMFCs becomes high since it is dependent on the price of platinum. It is not only the catalyst in a PEMFC which costs, as shown in Figure 9. Although, dependent on the production volume of a certain PEMFC-component, the price will typically decrease with higher volumes, except for the platinum catalyst since its price is largely determined by the price of the platinum raw material.[25] Therefore, also at high production volumes, the main factor influencing the price of a PEMFC is the use of platinum catalyst. Clearly, in order to make fuel cells economically competitive in comparison to other energy conversion devices, the cost of the catalyst has to be reduced.

Price reduction of the catalyst could in principle be done by making the use of platinum more efficient, however the dependency on the noble metal would still remain. In addition, it appears that the routes of improving the efficiency of platinum catalysts are close to exhausted. Another, perhaps more promising option, would be to develop inexpensive noble metal-free catalysts, with similar properties in terms of catalyst conversion efficiency and operation stability as the platinum-based catalysts. These types of catalysts are under development and will be discussed from now on throughout the rest of the thesis.

3.2 Development of noble metal-free catalysts

Over the last two decades, different strategies have evolved, developing noble metal-free catalysts, to overcome the use of platinum in PEM fuel cells. The three major classes of inexpensive noble metal-free catalysts are; *(i)* transition metal chalcogenides, *(ii)* functionalized carbon catalysts and *(iii)* transition metal-N_xC_y catalysts.

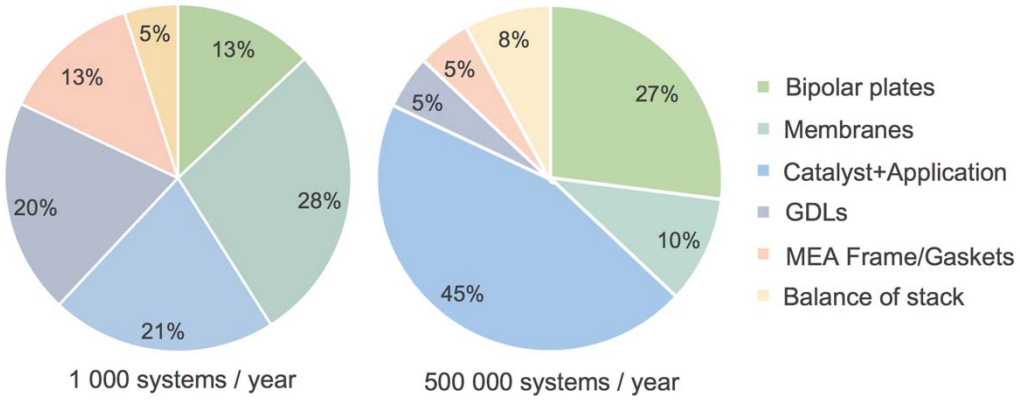

Figure 9. Predicted fuel cell stack cost contribution from various PEMFC components at two production volumes (2015). Reproduced from reference.[25]

3.2.1 Transition metal chalcogenides

The transition metal chalcogenides have developed noticeably over the last two decades.[26-29] Despite the progress, the activity of the catalysts can still not compete with the platinum based catalyst. However, the transition metal chalcogenides can at specific circumstances outperform platinum, since the catalyst is more resistive towards certain types of poisoning (such as methanol crossover) and this makes the transition metal chalcogenides attractive in particular applications for direct methanol fuel cells.[30-31]

3.2.2 Functionalized carbon catalysts

One major type of noble metal-free catalyst is the functionalized carbon catalysts; a metal-free catalyst which is commonly modified with nitrogen. These catalysts have shown remarkably high activity in alkaline fuel cells.[32-33] In acidic fuel cell conditions, the performance is not as high, although still substantial. Examples of modified carbons are; graphene, carbon nanotubes (CNT) treated in different ways to get functionality.[27, 34] In this thesis, functionalized carbons for acidic fuel cell conditions are relevant, since the catalysts studied in the thesis are as a combination of functionalized carbon catalysts and transition metal-N_xC_y catalysts.

3.2.3 Transition Metal-N_xC_y catalysts

Perhaps the most promising class of noble metal-free catalysts is the transition metal-N_xC_y catalysts (MeN_xC_y) catalysts. These catalysts basically consist of cheap elements such as carbon (C_y), nitrogen (N_x) and transition metals (Me); usually iron, but cobalt and nickel are also common. Already in the 60s, a class of non-precious compounds, phthalocyanines (shown in Figure 10a), were found to be ORR-active by Jasinski[35]. Later, other Me-N_x chelates with four nitrogens coordinating to a metal center, such as porphyrins (see Figure 10b), were also discovered to be electrocatalytically active.[36-37] A problem with these compounds were the stability for the oxygen reduction and it was discovered that heat treatment of the compounds improved their stability and in some cases, also their activity.[38-42]

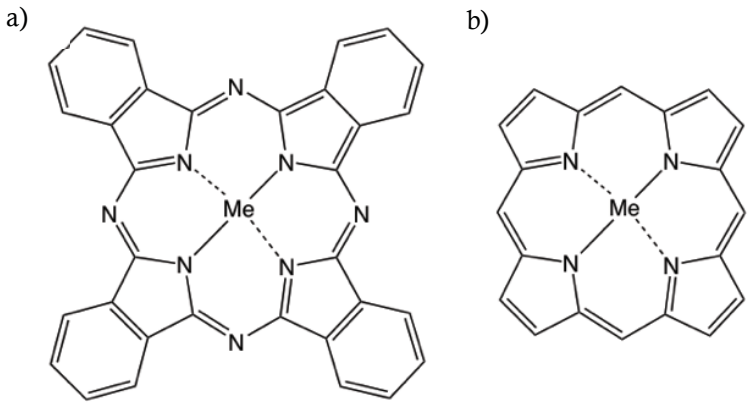

Figure 10. Chemical structures of (a) phthalocyanine and (b) porphyrin.

However, since these heterocyclic macrocycle organic compounds are also rather expensive, synthesis from simpler and cheaper molecules have developed. Consequently, several new promising catalyst materials with high ORR activity have been introduced in the last decade.[9-10, 43-51] Very simplified, it seems like mixing and heating of a number of compounds containing nitrogen, carbon and transition metals has the potential to give decent ORR-active catalysts.[52] The nature of the active site in these catalysts is debated;[26, 29, 53-57] however, most researchers agree on that the active site consist of an iron center coordinated by two to four nitrogens (not necessarily in a heterocyclic ring), incorporated in a carbon matrix.[27] A detailed function of these catalysts remains ambiguous and this is one of the main topics of this thesis. Even though the catalytic performance of these new noble metal-free catalysts is still inferior the platinum-based ones, they seem to have potential to compete with platinum-based catalysts and eventually replace this noble metal.

4. Our Approach for Designing New Catalysts

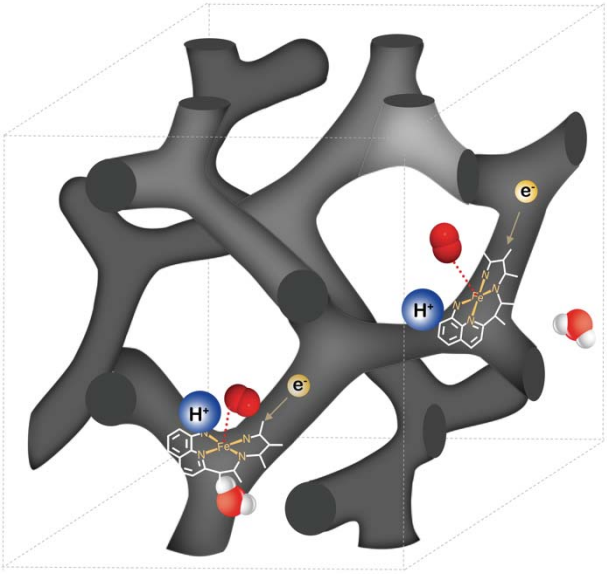

In this project, three requirements were strictly considered when designing new catalysts. The catalysts have to be *(i)* catalytically active for oxygen reduction and synthesized from *(ii)* cheap and *(iii)* abundant chemical elements. The project builds on the recently developed concept of the transition metal/iron ion-chelating ordered mesoporous carbons (TM-OMC/Fe-OMC).[9] Several studies have previously been done on this type of catalysts but the Fe-OMC catalyst type is still at an early stage of development and there are room for optimizations and improvements. To optimize the Fe-OMC catalyst further, different approaches can be used, although, the ultimate goal for each approach would be the same; to produce an as efficient and inexpensive catalysts as possible.

One approach, we chose in this thesis (and which Chapter 6 is dedicated to) is dealing with the fact of understanding the mechanism of the active site in Fe-OMCs catalysts. This is perhaps one of the most important and complex issues in the field. Another approach (dedicated to Chapter 7), deals with the synthesis/production of the catalysts with focus on improving the catalysts' carbon properties. This approach is more straight forward. By systematically changing parameters in the synthesis one could selectively track behaviours which are of advantage for the catalyst outcome. Changes in the synthesis route can also be done to eliminate unnecessary steps, making the process more efficient. Finally, in order to gain new knowledge about the catalysts, it is important to apply new theories/methods to describe and characterize the catalyst materials.

In the following part of this chapter, the idea and synthesis behind the Fe-OMCs are described. The importance of certain parameters will be explained, but weaknesses in the synthesis route will also be highlighted and where there is room for improvement.

4.1 Combination of important properties

An ideal (ORR) catalyst requires multiple properties such as highly active sites, high density of active sites, conductive capability and efficient mass transport properties. A challenge with catalyst materials is to combine all properties in one unity (see Figure 11). As mentioned previously high active site density and conversion efficiency can be achieved by using a catalyst support with large specific surface area. One way to achieve high surface area is to use porous structures.

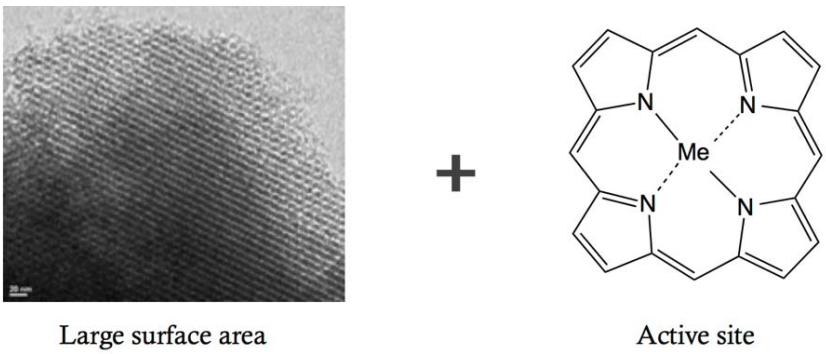

Figure 11. Schematic illustration of properties which have to be combined in the catalyst.

In this thesis, a hard template method in which an ordered mesoporous silica acts as a template for the formation of a porous carbon catalyst is used. The templating structure, and accordingly also the catalyst structure, is tunable and can be optimized for the desired system regarding mesophase (cubic, hexagonal, lamellar etc.), pore size and pore volume. The specific structure applied on the catalysts in this work is a bi-continuous ordered mesoporous cubic structure *Ia3d* (shown in Figure 12). The three-dimensional cubic structure is of advantage in the fuel cell since it facilitates mass transport of fuel gases and water in three directions. The silica template is synthesized using surfactants or block copolymers as structure directing agents which are thereafter removed by calcination. The silica template can then be impregnated with desired carbon precursors, pyrolized and etched away. The resulting material is the mesoporous carbon replica. High electrode area can be achieved by this use of a porous structure. An advantage of using an ordered porous structure is that the carbon formation and the establishment of the active sites are more likely to occur uniformly.

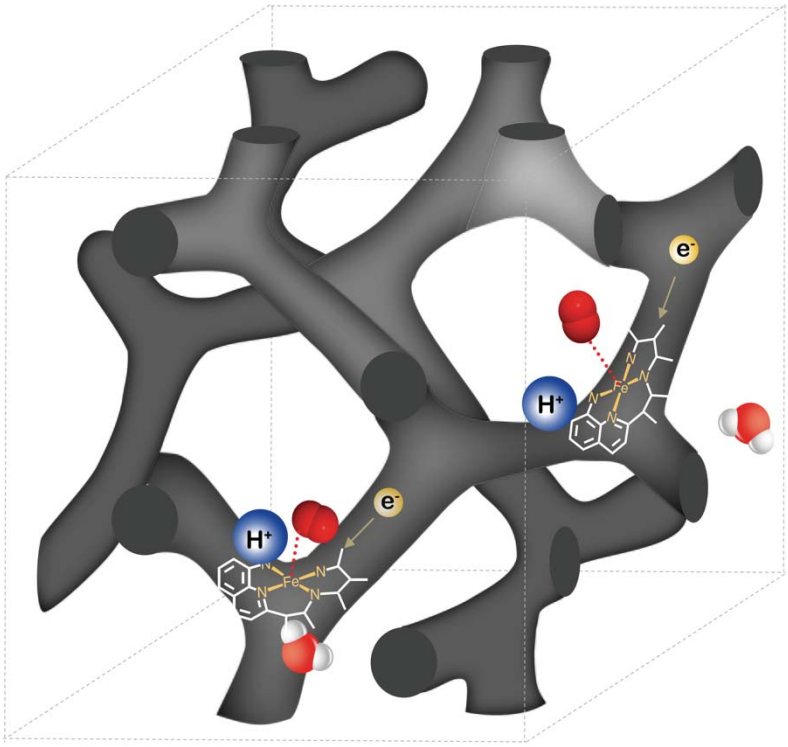

Figure 12. Schematic illustration of our iron-chelating ordered mesoporous carbon catalysts with a bi-continuous cubic ordered structure.

Many carbon materials are conductive and therefore a support based on carbon is suitable to attain conductive properties. However, the choice of carbon precursor and its crosslinking behaviors will most likely influence the conjugated system (and so also the conductivity) of the carbon structure. The type of carbon precursor will also influence the ability to replicate the silica template. It has to be liquid enough to impregnate the silica template, be reactive enough to succeed the cross-polymerization to form the porous structure and maintain its structure during the pyrolysis. The pyrolysis temperature will also highly influence the properties of the carbon. Clearly, many factors will influence the pore and surface properties of the carbon and are important to understand to achieve high conductivity, high surface area and efficient mass transport. More about these parameters will be discussed in Chapter 7 and Papers II and V.

However, perhaps the most important requirement the precursor mixture has to fulfill, is the ability to form ORR catalytic active sites. We believe that the precursor's capability to form iron-nitrogen chelates will influence the catalytic outcome, so the precursor composition and mixing parameters are important to consider (this will be discussed more in depth in Chapter 6). It is also essential that these iron-nitrogen chelates do not decompose during the pyrolysis and instead form active Fe-N_x-sites. To summarize, we want to incorporate active sites in an ordered mesoporous cubic carbon structure as illustrated in Figure 12.

4.2 Typical synthesis approach

The standard synthesis approach used in this work will now be presented and it may be useful to clarify concepts discussed in Chapters 6 and 7. Figure 13 shows a schematic picture of the steps in the synthesis procedure. Simply, the silica template is synthesized, impregnated with the carbon/nitrogen/iron precursor, heat treated, etched, where after the carbon catalyst can be obtained. To achieve better catalysts, one has to fine tune each of these steps in the synthesis route to enhance the best material properties and to eliminate unnecessary steps.

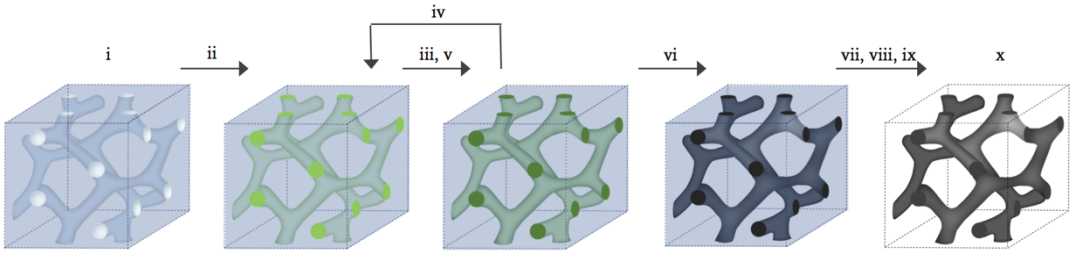

Figure 13. Schematic diagram of the synthesis procedure. (i) Ordered mesoporous silica (KIT-6) template, (ii) precursor mixing (furfurylamine + iron(III)chloride), aging, and first impregnation of template, (iii) first pre-heating step (100°C for 2 h in air), (iv) second impregnation, (v) second pre-heating step (160°C for 2 h in air), (vi) first pyrolysis treatment (950°C to 1100°C for 2h in nitrogen), (vii) silica template removal by HF or NaOH, (viii) sulfuric acid treatment, (ix) second pyrolysis treatment (950°C for 2 h in nitrogen), and (x) the final catalyst. Reprinted with permission from Paper I © The Royal Society of Chemistry 2018.

4.2.1 Precursor preparation and impregnation

The typical precursor solution is prepared from furfurylamine mixed with iron chloride, but other iron/carbon/nitrogen sources can also be used. The precursor solution needs to be liquid to be able to impregnate the silica template. Most likely iron-nitrogen chelates are formed during the precursor preparation which will influence the final catalyst performance. However, many factors seem to influence the chelate formations and will be discussed later in Chapter 6. The impregnation is a time-dependent process and sufficient of time is necessary to completely impregnate the silica. The impregnation is also dependent on the wetting properties of the precursor solution.

4.2.2 Crosslinking during heat treatment

The precursor impregnated silica undergoes two heat treatment steps (typically at 100°C and 160°C), which are necessary for crosslinking of the precursor. Complete crosslinking is needed to achieve a high surface area. Therefore, it is important to choose components in the precursor mixture which can crosslink. If the crosslinking instead is completed during the pyrolysis step

unwanted low surface area and larger pores seem to form.[9] The heat treatment may also influence the iron-nitrogen chelation.

4.2.3 Pyrolysis (Carbonization)

In the pyrolysis step the crosslinked carbon precursor in the silica template is transformed into carbon under inert atmosphere. This process is necessary to achieve conductive carbons. However, drastic changes in the carbon structure occur during the pyrolysis and prediction of these changes is very difficult. Few studies which correlate the carbon structure before and after pyrolysis have been made, perhaps because of lack of correlation, or more likely that it is difficult to investigate.

4.2.4 Silica template removal

The silica template is commonly removed by an acidic HF etch, which efficiently dissolves the silica template and keeps the active sites intact. However, HF is a very harmful and toxic chemical and should therefore be avoided. Other etch solutions should be considered and will be discussed later in Chapter 7.

4.2.5 Additional treatments

For most catalysts prepared in this thesis the additional treatment includes acid wash by sulfuric acid followed by a second pyrolysis. The purpose with the wash is to dissolve unwanted iron species which may block the porous structure and/or the active sites. However, the wash has to be chosen to not dissolve the active sites. A second pyrolysis is often performed following the sulfuric acid wash to get rid of sulphur species which may associate to the active sites and deactivate them.[10, 57-58]

4.2.6 The typical synthesis procedure and chemicals used

In a typical synthesis, mesoporous silica (KIT-6) is prepared (as described in [59]) and used as a template for preparing the mesoporous carbon catalysts. Furfurylamine and iron chloride are mixed and subsequently impregnated in the silica template and soaked overnight, followed by a heat treatment in air at 100°C for 2 h. A second impregnation is made, followed by a heat treatment in air at 160°C for 2 h. The sample is then pyrolized in an inert atmosphere at 950°C for 2 h. Thereafter, the silica template is removed by acid washing with 40% HF for 20 h at RT. Finally, an additional acidic treatment is made with 0.5M H_2SO_4 for 6 h at 80°C followed by another pyrolysis treatment in inert atmosphere at 950°C for 2 h. The main chemicals used in this thesis are presented in Table 1.

Table 1. The main chemicals used in the thesis, their suppliers and purities.

Chemical	**Supplier**	**Purity**
Furfurylamine	Sigma Aldrich	99%
Furfurylalcohol	Sigma Aldrich	99%
Anhydrous $FeCl_3$	Sigma Aldrich	>98%
Hexahydrated $FeCl_3$	Sigma Aldrich	>98%

5. Experimental methods and parameters

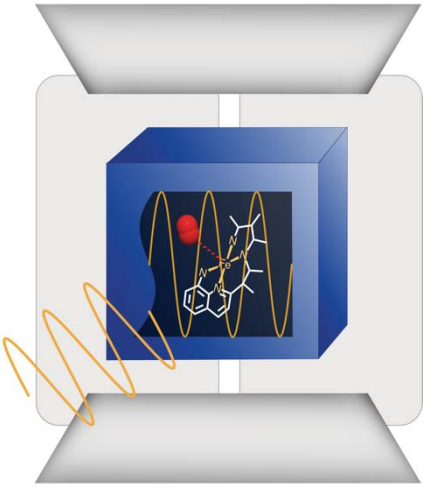

5.1 Methods used to study the active sites

Methods, such as X-ray Absorption Fine Structure (XAFS) and Mössbauer spectroscopy have been frequently used to achieve information about local atomic structures of the active sites.[9, 57, 60] Despite this valuable information, the detailed function of these catalysts remains ambiguous and more information is needed for a more complete understanding of the operating mechanism of the active sites. Therefore, alternative analytical methods should be considered. Two methods used in this thesis, mainly to get information about the active site, are briefly presented below.

5.1.1 Paramagnetic Nuclear Magnetic Resonance (NMR) Spectroscopy

Nuclear magnetic resonance (NMR) is a powerful method to study chemical structures of molecules. The method is based on the physical phenomenon that atoms which have an odd number of protons and/or neutrons in the nuclei have an intrinsic magnetic moment and an angular momentum which in an external magnetic field can absorb an electromagnetic wave. Dependent on the nuclei's chemical environment this absorption will occur at different wavelengths, which correspond to different chemical shifts.[61] The majority of the NMR measurements made in this thesis were made on samples containing unpaired electrons (different species of iron ions). The unpaired electron(s) will interact by a hyperfine coupling with the resonating nucleus affecting the NMR signal.[62] Because of this interaction it was possible in Paper I and II to determine how the furfurylamine is interacting with the paramagnetic iron ions in the precursor mixture, to what degree, and what was influencing this interaction. The iron ions will attract the electrons in the furfurylamine, which means that the protons in the furfurylamine will sense a larger effective magnetic field, shifting the protons' chemical shift downfield.[62] Paramagnetic materials also decrease the T_2 relaxation, which broadens the NMR signal. This phenomenon makes NMR on paramagnetic materials dependent on the concentration of the paramagnetic species in the sample. ^{1}H NMR spectroscopy measurements were conducted using a Varian 400 MHz spectrometer. Deuterated DMSO, contained in glass capillaries and inserted in the NMR-tubes, were used for reference.

5.1.2 Electron Paramagnetic Resonance (EPR) Spectroscopy

One method that has been less employed in this field is Electron Paramagnetic Resonance (EPR) spectroscopy. By EPR, species with unpaired electrons, such as some transition metal ions, can be identified and characterised. EPR can thus in principle be used simply as a tool to investigate the presence of coordinated iron ions in a catalyst. Moreover, in non-precious metal cathode carbon catalysts containing iron-nitrogen chelates, it is of interest to study the variations of such iron-nitrogen sites, the oxidation- and spin states of these sites, the electronic structure of the carbons, and the possible oxygen/active site-interaction within the catalyst. Very few focussed EPR studies have yet been published on this topic. [60, 63] This is likely in part due to that many of the non-precious metal catalysts developed are conductive, contain iron species and interact with paramagnetic dioxygen, all properties that tend to generate complex and broad EPR signals which are complicated to interpret. By systematic studies of our Fe-OMCs we believe we can contribute with new and additional information regarding the active sites. Electron paramagnetic resonance (EPR) spectroscopy measurements were conducted on 10 mg powder samples in quartz tubes using a Bruker Elexsys E500 EPR Spectrometer for 120 K and a Bruker EMXplus EPR Spectrometer for 5 K.

Like any other spectroscopic method, EPR spectroscopy probes the interaction between matter (the sample) and electromagnetic waves. According to Planck's law ($\Delta E=h\nu$), electromagnetic radiation will be absorbed if the energy difference between atomic or molecular states (ΔE) is equal to Planck's constant (h) times the frequency of the radiation (ν). In EPR, the sample is placed in an external magnetic field, B_0, to create a difference (ΔE) in the energy states of unpaired electrons.

All unpaired electrons have a spin angular momentum, S, which will cause a magnetic momentum. For electronic system with a spin state of S=1/2 the spin magnetic quantum number m_s are either -1/2 or +1/2. Because of the magnetic moment, the electrons will, when placed in the external magnetic field, B_0, align with or against the magnetic field. The electrons which magnetic moment is aligned with the field ($m_s = -1/2$) will end up in a lower energy state compared to the electrons with a magnetic moment aligned against the field ($m_s = +1/2$) and this phenomenon is called the Zeeman effect. The energy states are given by $E = \pm 1/2\, g\mu_B B_0$ where g is the g-factor and μ_B the Bohr magneton ($9.274\text{x}10^{-24}$ J/T). The g-factor is a proportionality constant which for many samples is equal to ~2 but it varies dependent on the unpaired electrons' electronic configuration. The g-factor can be calculated and used as a fingerprint to identify compounds. The two energy states linearly split as a function of the magnetic field as shown in Figure 14. By microwave irradiation of the electrons in the lower energy level (spin-down), they can absorb the radiation and make a transition to the higher energy level (spin-up). Absorption will occur when the energy of the electromagnetic wave (hv) is equal to the energy difference between the two energy states which results in the fundamental equation of EPR, see Equation 5.1. The energy difference is dependent on the electrons molecular environment but also on the external magnetic field B_0. The absorption of radiation gives rise to an EPR signal as shown in Figure 14.[64-66]

$$\Delta E = h\nu = g\mu_B B_0 \qquad [5.1]$$

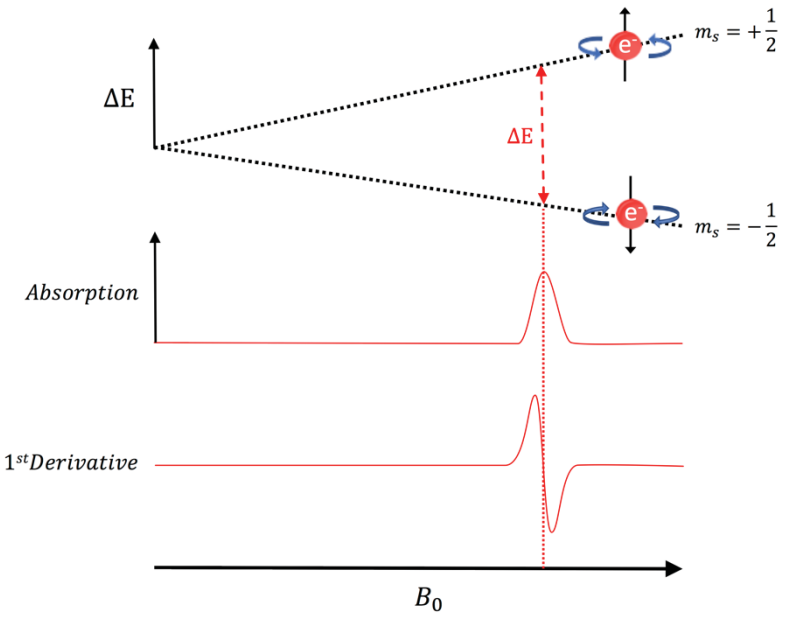

Figure 14. Variation of the spin state energies, the absorption and the first derivative of the absorption (the EPR signal) as a function of the applied magnetic field.

In EPR spectroscopy a *Spin Hamiltonian* is used to describe the magnetic interactions, of the unpaired electrons, with their specific environment. The Spin Hamiltonian (H) consists of a number of terms:

$$H = H_{EZI} + H_{ZFS} + H_{HFI} + H_{ESSI} \qquad [5.2]$$

Where H_{EZI} contributes with the Electron Zeeman Interaction of the electron spin with the external field, B_0, H_{ZFS} is the contribution from the Zero-Field Splitting in systems with $S \geq ½$, H_{HFI} comes from Hyperfine Interaction between electron and nuclear spins, and H_{ESSI} is the Electron Spin-Spin Interaction between electron spins on different nucleus. The theory behind the different spin Hamiltonian is rather demanding and will not be covered in this thesis.

5.2 Methods used to characterize the carbon structures

Several methods can be used to study material properties of Fe-OMC catalysts. The main characterization methods used in this thesis are described briefly below. Few other methods such as transmission electron microscopy (TEM), scanning electron microscopy (SEM), X-ray Photoelectron Spectroscopy (XPS), and contact angle measurements have also been used on the catalysts but these results are not included in the thesis.

5.2.1 Nitrogen physisorption

Nitrogen physisorption was used to gain information about the specific surface area, pore size, pore volume, micropore area, and pore size distribution in the catalysts. In a mesoporous material, the specific surface area can be calculated from the first adsorbed monolayer of nitrogen using the Brunauer-Emmett-Teller (BET) method.[67] By increasing the partial pressure of nitrogen, capillary condensation starts, causing an increase in the adsorption from which pore size and pore size distribution can be calculated with the Barrett-Joyner-Halenda (BJH) method.[68-69] Nitrogen physisorption measurements were done using a TriStar3000 instrument after degassing the samples at 225 °C for 4 h.

5.2.2 Raman spectroscopy

Raman spectroscopy is a technique based on scattering (inelastic and Raman) of monochromatic light, usually from a laser in the visible, near infrared, or near ultraviolet range. When exposing the material to the laser, molecular vibrations, phonons or other excitations in the material will interact with the laser light, shifting the energy of the laser photons up or downfield.[70] The shift gives information about the vibrational and rotational (low frequency) modes in the material which can be related to bond or structure types. In this thesis Raman spectroscopy was used to characterize vibrational modes and the nature of defects in the three-dimensional cubic meso-structured carbon used for the catalysts. Raman spectroscopy measurements were conducted on powder samples using an In-Via Reflex Renishaw Raman spectrometer. As the excitation source, the 532 nm line of an Ar-ion laser was used, which has a nominal power of 100 mW at the source. By using a diffraction grating with 2400 l/mm a spectral resolution better than 1 cm^{-1} could be achieved. Typically, Raman spectra were accumulated by 10 scans with a duration of 10 seconds

each. Raman spectra were recorded at RT. In order to compare the spectra of the different materials, the Raman spectra have been normalized to the baseline.

5.2.3 X-ray diffraction (XRD)

In X-ray diffraction, monochromatic X-rays are interacting with the material resulting in a scattering/diffraction pattern of the incident X-ray beam. Diffraction can only occur in crystalline (or partly crystalline) materials and information about the atomic arrangements in the material is achieved.[71] Herein, X-ray diffraction were used to investigate the degree of "graphitisation" of the Fe-OMC catalysts. X-ray Diffraction (XRD) measurements were conducted on powder samples using a Bruker D8 Advance instrument operated in Bragg-Brentano geometry using Cu Kα radiation.

5.2.4 Small angle X-ray scattering (SAXS)

Small angle X-ray scattering is another X-ray diffraction technique suitable for defining crystallinity and structural order at the meso length scale (2-50 nm).[72] In the thesis SAXS was used to identify the cubic order and determine the unit cell parameters of the Fe-OMC catalysts. Small angle X-ray scattering (SAXS) was done at beamline I711 at the MAX II ring of the MAX-lab national synchrotron laboratory (Lund, Sweden). The data were analyzed using the BioXTAS RAW program.

5.3 Electrochemical evaluation of the catalysts

5.3.1 Preparation of the Membrane Electrode Assembly (MEA)

A commercial Pt/C catalyst on a commercial gas diffusion electrode (10 wt% Pt/Vulcan with 0.5 mg Pt/cm^2 from Quintech) was used at the anode side. Commercial ionomer (Nafion® 115 or 112 membrane from Sigma) was used as proton conducting membrane. The as-received membranes were washed for 10-30 minutes in 3% hydrogen peroxide solution at 80 °C (diluted from 30% hydrogen peroxide solution, Merck), followed by 1 h activation in 0.5 M sulfuric acid at 80 °C (diluted from 38% sulfuric acid, Sigma Aldrich) and 3 times washed for 1 h in milli-Q water at 80 °C. Before and after each step, the membranes were washed with milli-Q water. Finally, and before the membrane electrode assembly the Nafion® membranes were sufficiently dried.

The cathode was prepared with two methods, where one of them is still under development. In the first and more established method (mainly used in this thesis) a cathode catalyst ink was prepared from well grinded Fe-OMC catalyst powder and Nafion® 117 solution (5 wt% Nafion in mixture of lower aliphatic alcohols and water from Sigma-Aldrich). The ink was well mixed thereafter applied (by hand with a pipette) on a gas diffusion carbon Paper (Toray Paper TGP-H-060 from Fuel Cell Earth). The final Fe-OMC/Nafion® (weight) ratio was 1.25 and the final Fe-OMC loading on the carbon Paper was in the range 5-7 mg cm^{-2}.[73]

In the second method, a cathode catalyst ink was prepared by mixing 0.2 g of propylene glycol (99% Sigma Aldrich), 1.65 g Nafion® D2021 solution (Fuel cell store), and 1 drop (about 0.02 g) of Dispersant KD2. Thereafter 0.5 g of the Fe-OMC catalyst powder was added and mixed with an ultrathurrax (Heidolph, Silent Crusher M) for about 2 min, followed by addition of 0.13 g

Vulcan XC-72R (Fuel cell store) and once again mixing with an ultrathurrax for about 2 min. The inks were screen printed with a Dyenamo DN-HM02 Laboratory screen-printer on Toray Paper TGP-H-060 (Fuel Cell Earth) as squares with the area of 2.56 cm^2. The printed catalysts were dried and then washed carefully in deionized water to remove the propylene glycol. The catalyst loading was about 3 mg cm^{-2}.

The assembly of the anode, cathode and Nafion® membrane was done with a hot press. First, the Nafion® membrane hot-pressed at 2 MPa and 135 °C for 60 s. Thereafter, the membrane and the anode were pressed together at 2 MPa and 135 °C for 60 s, and finally, the anode-membrane-cathode assembly was pressed at 2 MPa and 135 °C for 60 s. More detailed parameters for the MEA preparation are given in the cited reference.[73]

5.3.2 Single cell PEM fuel cell measurement

Electrochemical evaluations of the MEA were made in a commercial 5 cm^2 single cell PEM fuel cell from Scribner Assoc. using an electrode area of 2.56 cm^2. The measurements were done at 80 °C. The cell was fueled by fully humidified 100% H_2 (instrumental grade from AGA) and using synthetic air (instrumental grade from AGA) as a fully humidified oxidant. A total back-pressure of 1.5 bar was applied at both the anode and cathode side of the cell. Polarization curves were measured for each catalyst in cycles (cyclic voltammetry) with a Gamry (Reference 600) potentiostat. The potential was held at the open circuit potential for 300 s before the cyclic voltammetry. To verify variations in resistance in different catalysts *electrochemical impedance spectroscopy* (EIS) was used. Electrochemical impedance measurements were done in the single cell at 0.7 V between 100 kHz und 0.01 Hz with 10 measurement points per decade.

5.3.3 Rotating Disk Electrode measurements

Rotating disk electrode (RDE) measurements were carried out using a three electrode RDE setup from Gamry Instrument in 0.1 M $HClO_4$ solution. $Ag/AgCl_{sat}$ and a graphite rod (6 mm diameter) served as reference and counter electrode, respectively. The catalyst inks were prepared by ball milling the catalyst for 40 min (15 Hz), followed by mixing 10 mg catalyst, 95 µL Nafion® solution (5 wt% in lower aliphatic alcohols and water, Sigma-Aldrich) and 350 µL ethanol (99.5 % Solveco). After sonication (30 min) 5 µL of the ink was deposited on a polished glassy carbon rotating disk electrode (5 mm diameter, Gamry Instrument) and dried in room temperature for 30 min. The ORR polarization curves were recorded stepwise, every 30 mV, with a hold time of 60 s, starting at 1 V to -0.25 V (versus RHE) in oxygen saturated electrolyte. The potential was held at the open circuit potential for 120 s before every polarization experiment. A polarization curve was measured for each catalyst at four different rotation speeds (100, 400, 900 and 1600 rpm). To achieve the Koutecky-Levich plots the Koutecky-Levich equations[74] presented below were used:

$$\frac{1}{i} = \frac{1}{i_L} + \frac{1}{i_K} = \frac{1}{Bw^{1/2}} + \frac{1}{i_K} \qquad [5.3]$$

$$B = 0.62nFAC_0{D_0}^{2/3}v^{-1/6} \qquad [5.4]$$

Here, i_L is the diffusion limited current and i_K the kinetic current. The coefficient used to calculate the number of electron transfer mechanism for each catalyst was obtained from the Faraday constant (F=96485 mol^{-1}), the electrode area (A=0.196 cm^2), the bulk concentration of O_2 in 0.1 M

$HClO_4$ (C_0=1.2x10^{-3} mol L^{-1}), the diffusion coefficient of O_2 in 0.1M $HClO_4$ (D_0=1.93x10^{-5}cm^2 s^{-1}), and the kinetic viscosity in $HClO_4$ (ν=0.00893 cm^2 s^{-1}).

6. The active site – the heart of the catalyst

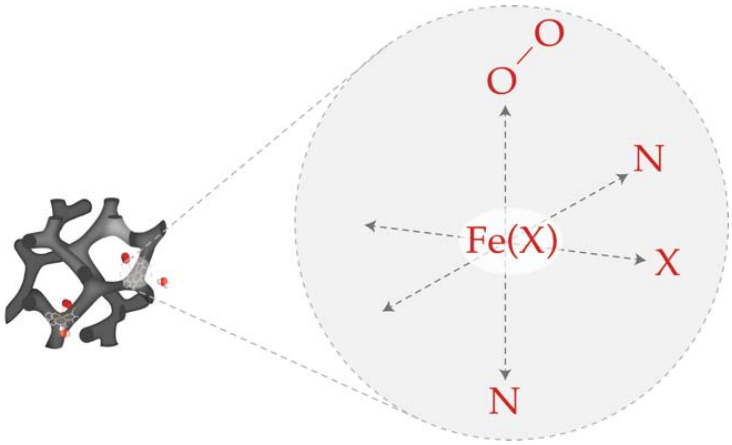

In the field of non-precious metal cathode catalysts, understanding the structure and function of the active sites is central to further develop active and durable catalysts. To shortly illustrate the importance of understanding the active site in MeN_xC_y catalysts, we will look into the function of the *heme* molecule (illustrated in Figure 15). Heme, a segment of the protein haemoglobin, is vital in the transport of oxygen to our cells. The molecule consists of a porphyrin, with an iron ion coordinated to the center. The iron center provides a site for an oxygen molecule to coordinate/bind, whereupon it is transported through the body (via the blood) to the cells. When the oxygen enters a cell it finally disassociates from the site and is consumed. The iron-oxygen coordination can only happen if the oxidation state of the iron is +II.[75-77] When the oxygen binds, it temporarily oxidizes iron (+II) to iron (+III) and becomes a superoxide ion. If the superoxide ion is protonated, the iron will remain oxidized and incapable of binding more oxygen. The complex coordination geometry will vary if the iron site binds to an oxygen (by a covalent bond) or to a water molecule (by a co-ordinate bond). The oxygen pulls the iron (+II) into the plane of the porphyrin ring, causing a conformational change. Despite the fact that the ORR mechanism is different, the heme example illustrates important properties of a MeN_xC_y catalyst. The oxygen has to bind strong enough to be attracted to the active site but weak enough the be able to dissociate in a later step. In the MeN_xC_y catalysts, the active site offers a site for electrons, protons and oxygen to meet and react. The ORR activity seems to be highly influenced by the oxidation state of the iron and depends on the ligands coordinated around it. We found many of these properties important to study for our ORR catalyst and are therefore investigating methods which can give us this information such as electron paramagnetic resonance spectroscopy.

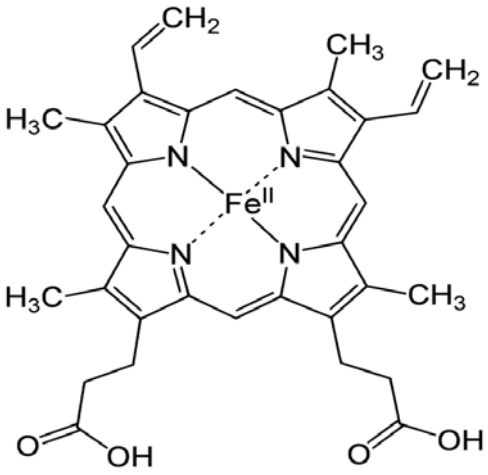

Figure 15. Molecular structure of heme.

6.1 The active sites of previously studied Fe-OMCs

The local atomic structure around the iron in the Fe-OMC catalysts has previously been studied with Extended X-ray Absorption Fine Structure (EXAFS) to identify the active sites. Fe-N_x and O_2-Fe-N_x chelates were proposed to be responsible for the main catalytic activity.[10] These results have provided a reasonable understanding of the structure of Fe-N_x active sites, but there is still need for more complete information.

6.2 Influence of nitrogen in the precursor on the catalytic activity

In Paper II, we wanted to investigate the influence of nitrogen in the precursor on the catalytic performance of the catalyst prepared. As mentioned, previous EXAFS studies on Fe-OMC catalysts, suggest that the active site consists of iron-nitrogen (Fe-N_x) chelates bound to the carbon matrix [10]. However, to distinguish between Fe-N_x and Fe-O_x bonds with EXAFS is difficult. To eliminate the Fe-O_x bond as an option we wanted to test the necessity of including nitrogen in the formation of the Fe-OMC and determine its role in the active site. This was done using two derivatives of furan as precursor; one containing nitrogen (furfurylamine) and one nitrogen-free (furfurylalcohol). Furfurylamine has an amine-group as functional group whereas the corresponding functional group in furfurylalcohol is an alcohol-group as shown by the molecular structures in Figure 16 (red and blue, respectively). The two reactants were also mixed with an iron source to enable formation of chelates.

From electrochemical evaluation it was clear that nitrogen has a crucial role in the formation of the active sites. This was evident in the very poor fuel cell performance for the nitrogen-free catalyst (**FuOH-Fe**) compared to the behavior of the nitrogen containing catalyst (**FuNH$_2$-Fe**), see Figure 16. The higher catalytic activity achieved in the **FuNH$_2$-Fe** catalyst implies high concentration of active sites, whereas the low activity for the **FuOH-Fe** catalyst indicates only few, or no, active sites. EPR studies of these materials were also performed and will be discussed more in depth in Section 6.6.1. The results in the study strengthen previous theories[9-10] that the nitrogen is involved in the formation of active sites in Fe-OMC catalysts.

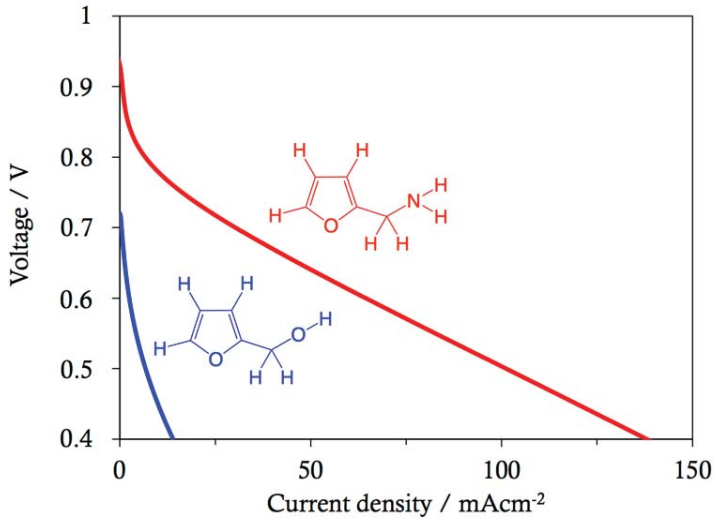

Figure 16. Fuel cell polarization curves of FuNH$_2$-Fe (red) and FuOH-Fe (blue). Reprinted with permission from Paper II © 2017 American Chemical Society.

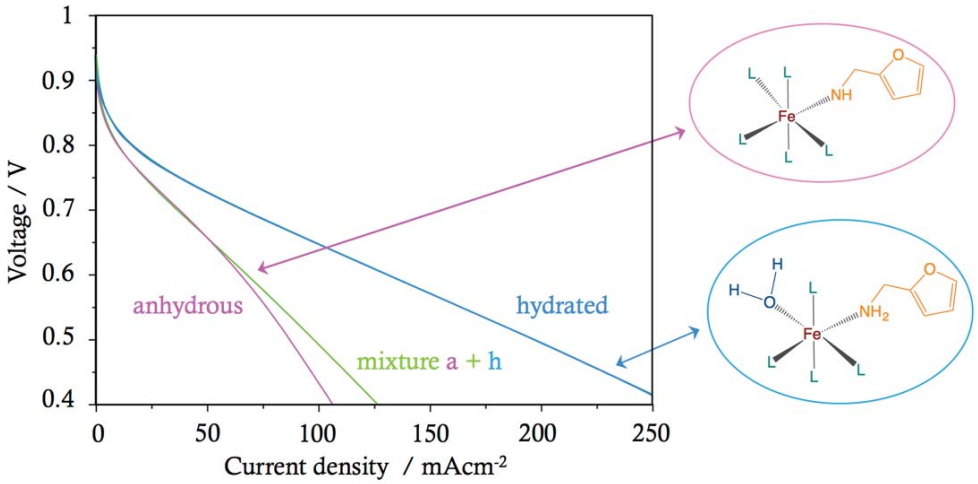

Figure 17. Fuel cell polarization curves of Fe-OMC catalysts prepared with precursor solutions using various iron sources (anhydrous $FeCl_3$ – magenta, hydrated $FeCl_3$ – dark cyan, anhydrous $FeCl_3$ + hydrated $FeCl_3$ (molar ratio 50%) – light green.

6.3 Influence of iron precursor hydration state on the catalytic performance

As discussed in both Papers I and II, we believe that iron in combination with nitrogen form chelates which are responsible for the formation of active sites. Many parameters likely influence the formation of these chelates such as the type of N/C-precursor and the type of transition metal.[9] In Paper I it was discovered that the hydration state of the iron chloride precursor used has a large impact on the catalytic activity of the synthesized catalysts. The catalyst made from hydrated $FeCl_3$ had a significantly higher performance compared to the catalyst made from anhydrous $FeCl_3$, as shown in Figure 17.

In the same study, it was also found that the aging time after mixing of the precursors and the relative amount of iron to N/C-precursor used during synthesis also influence the catalytic performance. To better understand the chemical difference between the precursor mixtures based on anhydrous $FeCl_3$ or hydrated $FeCl_3$ ^{1}H-NMR spectroscopy was used. Differences in the proton shifts of furfurylamine was observed depending on whether the precursor mixture was made by anhydrous $FeCl_3$ or hydrated $FeCl_3$, indicating different type of complex formations in the two cases. It was observed that the amine group in the furfurylamine molecule is closest to the iron in the iron-nitrogen chelates as shown in Figure 18 and that water in the hydrated $FeCl_3$ likely competes with the furfurylamine to be closest to the iron site.

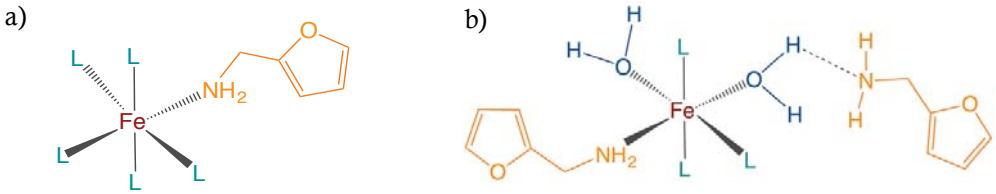

Figure 18. Schematic representations of furfurylamine interacting with the iron (left) and of the competing iron-ligand interactions between water and furfurylamine. L represents either a ligand coordinated to the iron or a vacant coordination site of the iron. Reprinted with permission from Paper I © The Royal Society of Chemistry 2018.

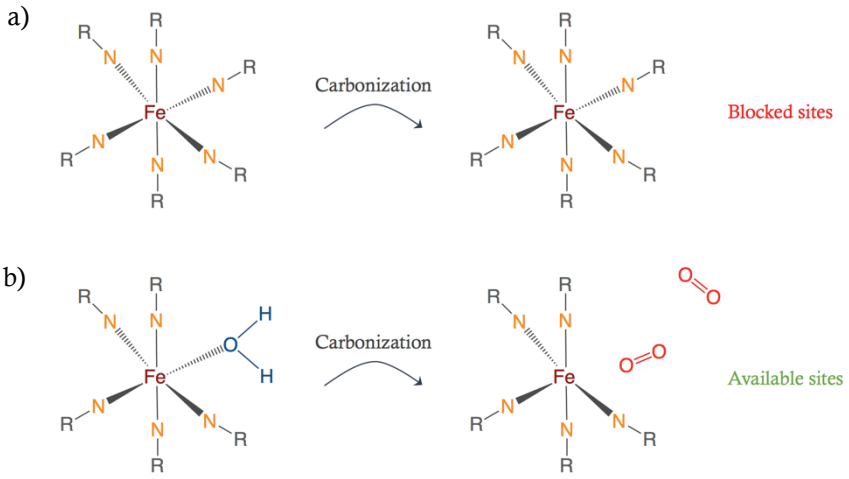

Figure 19. Schematic illustration suggesting that a too high iron-nitrogen coordination may block the access of oxygen to the active site (a) whereas lower iron-nitrogen coordination may leave open available sites (b).

It was also found that the precursor aging time and the iron to N/C-precursor ratio also had a significant impact on the complex formation and the degree of furfurylamine-iron coordination in the precursor mixtures. Since the three parameters; *i)* hydration state of $FeCl_3$, *ii)* precursor aging time and *iii)* iron to N/C-precursor ratio, had an impact on both the complex formation and the activity of the Fe-OMCs, a correlation between the two could possibly be found. It is clear that some iron-nitrogen coordination is necessary to form active sites, but too high iron-nitrogen coordination appears to be unfavorable and to limit the access for oxygen to the iron, thereby lowering the ORR activity as schematically illustrated in Figure 19.

6.4 Correlations between the precursors' iron-nitrogen interactions and the catalysts' active sites

In both Paper I and II we observed that iron-nitrogen interactions in the precursor solution can be correlated to the catalytic activity in the final catalyst. This opens up possibilities to screen potential metal/N/C-precursor combinations in a very early stage of the synthesis. Time and cost wise this would be of great advantage, since poor catalyst precursors could be identified early on without having to complete the whole synthesis. Few studies have discovered correlations between sample properties before and after pyrolysis. Instead, the pyrolysis process is known to drastically change the structure of MeN_xC_y catalysts.[10, 78] Though, what is shown in Paper I is that the paramagnetic shift can be used to identify and, to some extent quantify chelate interactions, which can potentially serve as tool to identify an optimal interaction resulting in a maximized active catalyst.

To further prove that the initial iron-nitrogen interaction achieved before polymerization and pyrolysis plays a role for the catalytic activity, we can consider results from Paper II. Two catalysts were prepared out of precursor mixtures consisting of half (molar) amount of furfurylamine and half furfurylalcohol with $FeCl_3$. The two samples were prepared with reverse mixing orders of the amine and alcohol. In the first sample the amine was first mixed with the $FeCl_3$ and subsequently mixed with the alcohol (**$FuNH_2$-Fe-FuOH**) and in the other sample the opposite procedure was done (**FuOH-Fe-$FuNH_2$**). Different ORR activity was obtained and this is most likely because of

interactions between nitrogen and iron take place already in the precursor phase and will influence the active sites formed in the catalysts. We hope to develop this idea further in the future and to confirm that the nitrogen-iron interaction before the pyrolysis step is crucial in order to form ORR active Fe-OMC catalysts.

6.5 Influence of iron precursor anion on the catalytic performance

We have already seen that the hydration state of the iron chloride precursor influences the final activity of the Fe-OMC catalysts. Naturally, it is analogous to think that also the type of iron precursor salt would influence the catalysts activity. Therefore, in Paper IV we studied the influence of iron salt with focus on the iron salts' anions. The idea was to use organic-soluble anions to increase the solubility of the iron salts in the N/C precursor (furfurylamine). With the increased solubility, the goal was to increase the iron loading and the number of active sites in the final Fe-OMCs and consequently enhance the catalytic activity. The three additional iron salts, except for the commonly used *iron(III) chloride hexahydrate* (Figure 20a), were *iron(II) acetate*, *iron(II) tetrafluoroborate hexahydrate*, and *iron(II) trifluoromethanesulfonate* (Figure 20b-d). As expected the solubility of the iron salt in furfurylamine was radically increased. However, the iron concentration in the final Fe-OMC catalyst was only increased for one of the samples (OTf-Fe-OMC) shown in the elemental analysis data in Table 2.

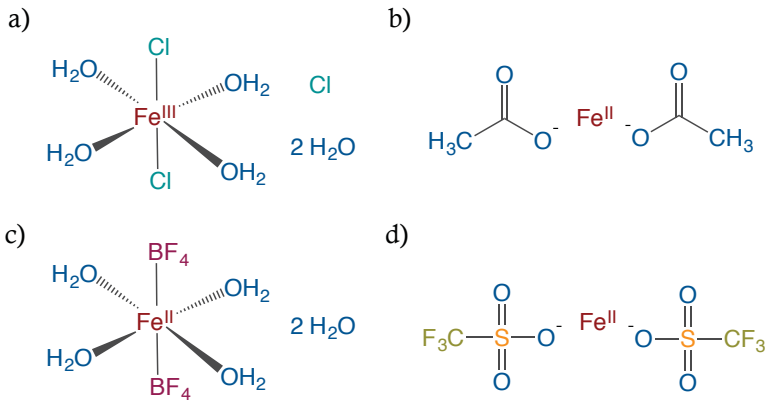

Figure 20. Molecular structures of (a) iron(III) chloride hexahydrate, (b) iron(II) acetate, (c) iron(II) tetrafluoroborate hexahydrate, and (d) iron(II) trifluoromethanesulfonate.

Table 2. Iron loading in the Fe-doped OMCs.

Fe-OMC catalyst	**Iron loading (wt%)**
Cl-Fe-OMC	0.4
OAc-Fe-OMC	0.11
OTf-Fe-OMC	3.88
BF4-Fe-OMC	0.46

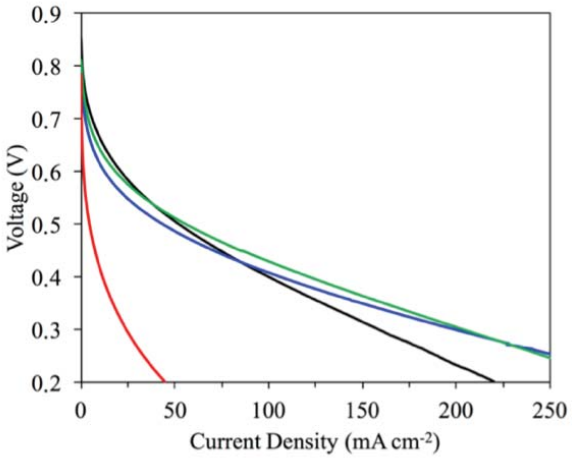

Figure 21. Fuel cell (left) and RDE (right) polarization curves (left) for Cl-Fe-OMC (black), OAc-Fe-OMC (red), OTf-Fe-OMC (green), and BF4-Fe-OMC (blue) from Paper IV.

Unexpectedly, the OTf-Fe-OMC catalyst (with increased iron loading) did not show an increased catalysts activity for the reduction of oxygen in the fuel cell (and rotating disk electrode experiments in Paper IV) as shown in Figure 21. This suggests that the main fraction of the iron in the sample consist of inactive iron species (or less active species) compared to the iron species in samples Cl-Fe-OMC and BF4-Fe-OMC. To identify differences between the samples and gain insight into the nature of the iron species, EPR spectroscopy were used. In conclusion we can say that the use of different iron salts may not necessarily increase the iron loading in the Fe-OMCs or their performance in PEMFCs, but it does influence the *type* of iron species formed.

6.6 EPR spectroscopy on Fe-N/C catalysts

A large portion of this thesis work has been focused on learning and establishing EPR spectroscopy as a method to study Fe-OMC catalysts and eventually other Fe-N/C catalysts. The purpose with using EPR to study Fe-N/C catalysts was to gain a better understanding of the types of iron species the Fe-OMC catalysts consist of and identify the ORR-active sites. Inconveniently, EPR on Fe-N/C catalysts is not instantly straight forward, because the materials are conductive, contain iron species and interact with paramagnetic dioxygen, all properties that tend to generate complex and broad EPR signals. To overcome some of the complications, we propose in Paper V, a few different sample treatment methods useful to simplify the interpretation of the EPR signals. In Paper V, six EPR signals were identified and they are summarized in Table 3. With these in mind we will in the following section extend the discussion about these signals and their origin to help understand the importance of the EPR study.

6.6.1 Sample treatment methodology

The first experiments completed with EPR spectroscopy on the Fe-OMC catalysts did not show very promising results with very noisy data. Luckily, the experiments were continued and by finding the right measurement conditions and instrument parameters, multiple EPR-signals could finally be observed in the Fe-OMCs. In Paper V, we describe a number of external parameters influencing the EPR signals of a Fe-OMC sample, including ball milling the sample, diluting the sample in a diamagnetic matrix, measurement temperature, and measurement atmosphere. It is important to be aware of these parameters, otherwise spectral information may not be observed.

Table 3. Summary of the identified EPR signals from Paper V.

EPR signal	Magnetic field (Gauss)	g-value	Shape	Origin
O signal	3370	2.00	sharp	Oxygen radical (Superoxide ion)
R signal	1585	~ 4.25	broad	Iron(III) species: Rhombic (S=5/2) or axial (S=3/2)
R2 signal	~ 3255	~ 2.07	broad	Axial iron(III) species (S=3/2) or oxygen radical
F signal	0-1500	-	broad	Iron(II) species (S=2)
S signal	~ 3240	~ 2.08	broad	Superparamagnetic particles
C signal	2000-4000	-	broad	Delocalized electrons in conductive carbon matrix

In Paper II, EPR spectroscopy was used to identify iron coordination in the nitrogen containing catalyst (**FuNH$_2$-Fe**) and absence of iron coordination in the nitrogen-free catalyst (**FuOH-Fe**). Several EPR-features were detected in the spectrum of the nitrogen containing catalyst compared to only a small feature in the spectrum of the nitrogen-free catalyst. The features in the nitrogen containing catalyst indicated coordinated iron in the structure whereas the absence of features in the nitrogen-free catalyst validated the absence of iron coordination. Unfortunately, at the time when Paper II was written, we were not aware of all external factors influencing the spectra described in Paper V. It should be mentioned that the as-prepared **FuNH$_2$-Fe** and **FuOH-Fe** samples showed very different morphology, where the **FuOH-Fe** sample consisted of relatively large aggregates. According to Paper V large aggregates are expected to provide lower microwave penetration as well as higher conductivity. This was evident by the difficulty to tune the microwave cavity and the low Q-factor for the **FuOH-Fe** sample. Consequently, the two samples were ball milled and EPR experiments were performed once again. In Figure 22, the as-prepared samples (lower trace) are compared to the ball milled samples (upper trace). What was previously interpreted as absence of EPR-signal in the **FuOH-Fe** sample was clearly a misconception, since the sample after ball milling showed at least two visible broad EPR-signals. The conclusion in Paper II will not change drastically since the EPR-signals in the ball milled **FuOH-Fe** sample are not consistent with the EPR-signals in the ball milled **FuNH$_2$-Fe** sample. By cooling the **FuNH$_2$-Fe** sample (see Figure 23), the ***F***, ***R*** and ***O*** signals can be detected, which might have a relation to the activity of the catalysts according to Paper V. In the **FuOH-Fe** sample however, one of the

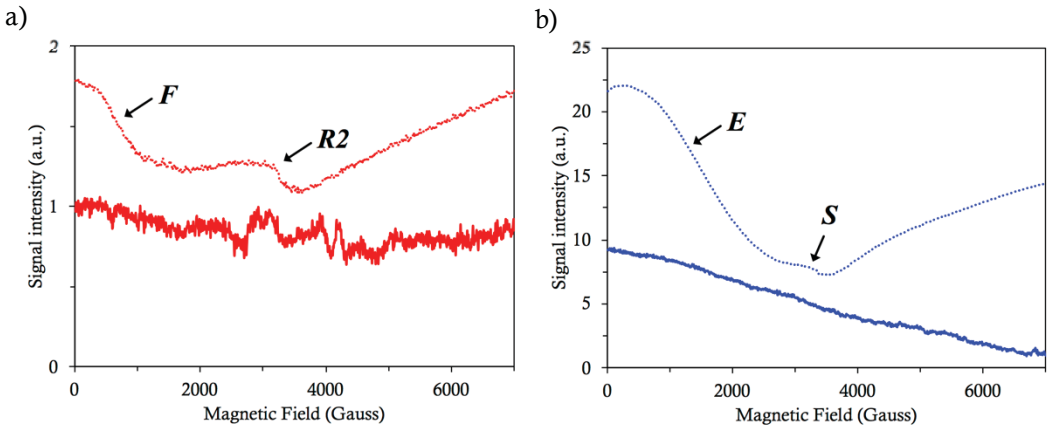

Figure 22. EPR spectra of as-prepared (lower trace) and ball milled (upper trace) FuNH$_2$-Fe (red) and FuOH-Fe (blue) catalysts collected at 295K in air.

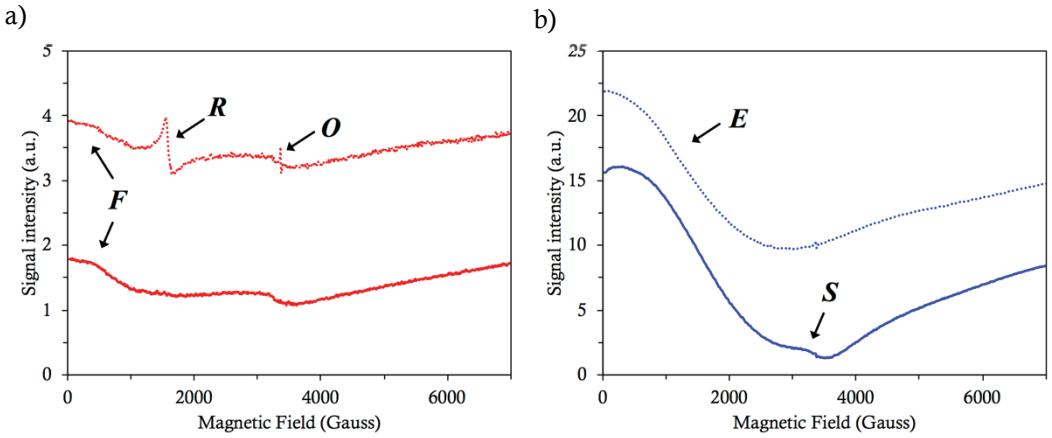

Figure 23. EPR spectra of ball milled FuNH$_2$-Fe (red) and FuOH-Fe (blue) catalysts collected at 295K (lower trace) and 180K (upper trace) in air.

previously observed signals was the ***S*** signal identified, caused by inactive magnetic nanoparticles.[79] Furthermore, a "new" signal, denoted ***E***, which was not found in Paper V was identified. The ***E*** signal, (should not be confused with the ***F*** signal) is a broad signal (0-3000 Gauss) which could be related to ferromagnetic resonance from elemental iron.[80] It should also be mentioned that the color of the **FuOH-Fe** sample was slightly greyish which is in agreement with elemental iron in the samples. To conclude the EPR-experiments from Paper II, the absence of EPR-signals in the as-prepared **FuOH-Fe** sample was not due to absence of iron coordination. The absence was due to difficulties to observe EPR signals in the sample's as-prepared state. After ball milling the **FuOH-Fe** sample, EPR signals were observed, which we conclude are not related to any ORR-active species.

6.6.2 EPR to identify differences in Fe-OMCs

Even though extensive information about iron species can be gained with EPR, the method can also be used as a simple screening method to identify differences in Fe-OMC samples. In Paper IV, EPR was clearly useful to identify differences in the Fe-OMCs prepared with different iron salts. The EPR-results showed (see Figure 24) that the use of different iron salts definitively

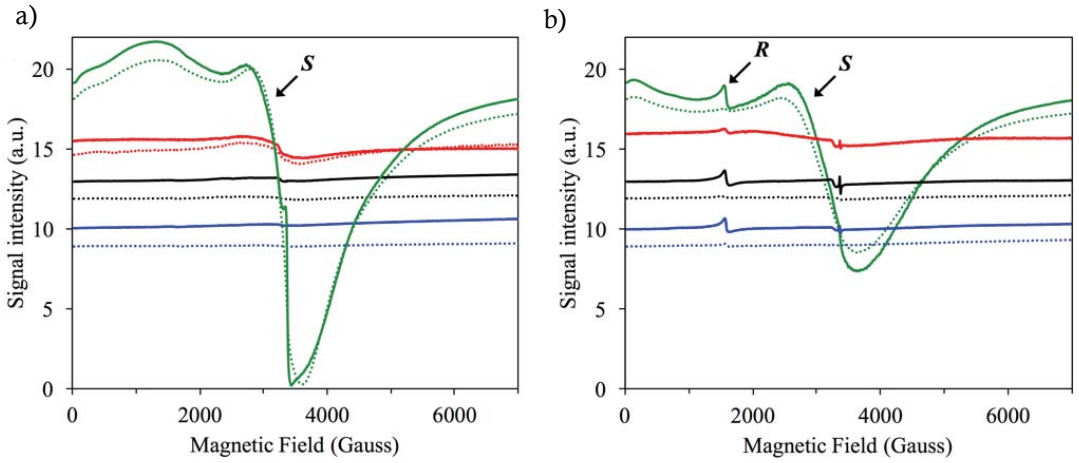

Figure 24. EPR spectra of Cl-Fe-OMC (black), OAc-Fe-OMC (red), OTf-Fe-OMC (green), and BF4-Fe-OMC (blue) collected at 295K (a) and 120K (b) in air (solid line) and in nitrogen atmosphere (dotted line).

influences the formation of different iron species in the Fe-OMC catalysts where the OTf-Fe-OMC sample showed a remarkably different EPR-signal compared to the other samples in the study.

6.6.3 EPR on iron chelates with oxidation state +II and +III

As previously described EPR spectroscopy can be used to detect unpaired electrons. Therefore, when studying Fe-OMCs with EPR it is of high importance to understand the Fe-OMCs' ability to form unpaired electrons and if so the possible molecular environment for these unpaired electrons. We already know that the main active sites in Fe-OMC catalysts have been identified to consist of iron ions interacting with nitrogen and oxygen containing ligands (as Fe-N_x and O_2-Fe-N_x chelates) in a carbon lattice. In an iron-ligand complex, the ligands' geometry (around the iron site) and ligand strength will depend on the ligand-orbitals interaction/overlap with the *d*-orbitals of the iron ion. The orbital interactions will lead to splitting of the *d*-orbitals' energy states. Figure 25 illustrates splitting patterns of the *d*-orbital energy states for a few common ligand coordination geometries and the patterns are dependent on the ligands around the transition metal ion.[81]

In Figure 26, the possible electron configurations in the five *d*-orbitals are specified for the two most common oxidation states of iron (+II and +III). Iron in oxidation state +II, and +III, have 6, and 5 electrons, respectively, distributed in their *d*-orbitals. In the figure the energy levels for the different *d*-orbitals are placed on the same energy level for simplicity and since the ligand geometries are at this point unknown. The splitting of the *d*-orbitals will affect the spin states of the iron ions which in turn will influence the formation of unpaired or paired electrons. As can be observed in Figure 26, the irons with oxidation state III, contain unpaired electrons in all spin states meaning that all species should be detectable by EPR. For the irons with oxidation state II, unpaired electrons can only be found in the high spin states (S=1 and 2). This means that iron sites in Fe-OMCs (active or inactive) with iron(II) centres with low spin are not detectable by EPR.

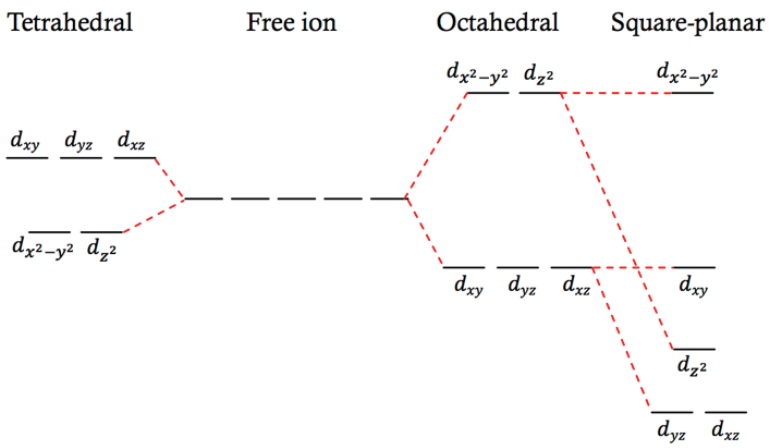

Figure 25. Schematic illustration of energy levels of the d-orbitals in common stereochemistries.

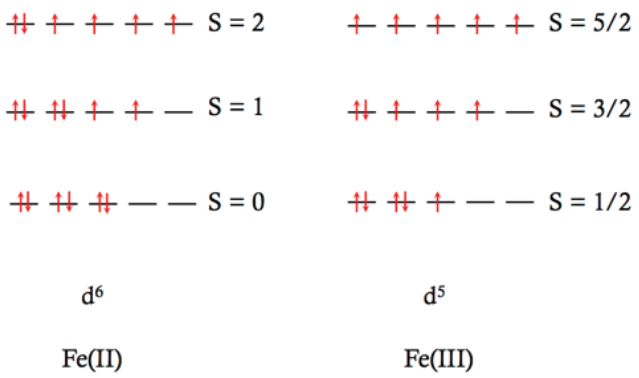

Figure 26. Schematic illustration of possible electron configurations in the five d*-orbitals for iron(II) and iron(III), the energy levels are placed on the same energy for simplicity.*

As visible in Figure 26, an iron ion can contain between 0 and 5 unpaired electrons, and the number of electrons involved and the corresponding spin states will have a significantly different influence on the EPR spectra. One can assign EPR spectra in two classes. The first class includes spin centers with an odd number of unpaired electrons and thus half-integer spin (referred to Kramers centers). In zero field (absence of magnetic field), half-integer spin states will always form degenerate doublets. When magnetic field is applied the doublets split linearly with the field strength and the resonance condition becomes $\Delta E = h\nu = g\mu_B B_0$ as previously described in Section 5.1.2. The second class includes spin centers with an even number of unpaired electrons and thus integer spin states (referred as non-Kramers centers). For integer spin states, the spin states in zero magnetic field may have different energies and there is no guarantee that two spin levels end up at the same energy level (as a degenerate doublet) as in a Kramer system. The zero-field splitting in integer spin systems causes the appearance of the EPR to fundamentally change compared to EPR spectra of half-integer spin systems.[64, 82]

6.6.4 The active sites in previously studied Fe-N/C catalysts

As mentioned in Section 3.2.3 the active site structure of Fe-N/C catalysts have been highly debated. Several studies (made by Kramm et. al.) have used Mössbauer spectroscopy to identify the active sites of Fe-N/C catalysts.[57, 83-84] Especially two iron species have been identified and correlated to ORR activity, which are the $Fe^{II}N_4/C$ with low spin and N-$Fe^{II}N_{2+2}/C$ with high

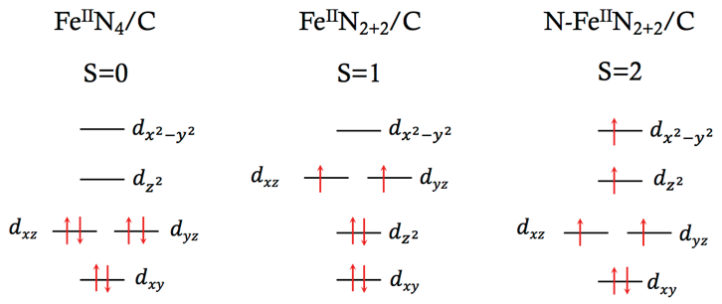

Figure 27. D-orbital energy schemes and electron configurations of $Fe^{II}N_4/C$ (S=0), $Fe^{II}N_{2+2}/C$ (S=1), and N-$Fe^{II}N_{2+2}/C$ (S=2). Reproduced from reference.[57]

spin (S=2). The species $Fe^{II}N_{2+2}/C$ with intermediate spin (S=1) was also found but identified as ORR-inactive. The inactivity in this species was believed to be due to the filled d_{z^2}-orbital (see Figure 27) preventing end-on adsorption of molecular oxygen compared to the active sites with an empty or single electron occupied d_{z^2}-orbital allowing dioxygen to adsorb, initiating the reduction of oxygen. Other species identified as inactive was $(N\text{-}Fe^{III}N_4)\text{-}O_2/C$, the high spin $XY\text{-}Fe^{II}N_4/C$ and magnetic particles of possibly iron nitride.

The synthesis of the Fe-N/C catalysts made by Kramm et. al. is rather different to the synthesis of Fe-OMC but it is not unlikely that the two catalysts have relatively similar active sites. It is of high interest to measure the Fe-OMCs with Mössbauer spectroscopy, but the Fe^{57} enriched iron(III) chloride is rather costly and the focus has instead been on understanding the iron species in our Fe-OMC catalysts with EPR spectroscopy.

6.6.5 EPR signals in Fe-OMCs which could be related to the activity

In all catalysts, that have shown any oxygen reduction activity (in Paper II, III, IV, and V), the EPR signals ***F***, ***R***, ***R2*** and ***O*** have been found. This fact does not explicitly mean that the signals originate from, or are related to, active site species, but the signals must definitively be investigated further. One should be careful to correlate ORR activity directly to an EPR signal. As was discussed in Paper V, it is possible that samples which do contain a large number of active sites, show relatively low ORR activity because of poorer carbon matrix properties. One of the highly interesting signals observed in the Fe-OMCs is the **F** signal. Signals with similar shape as the **F** signal have previously been found in iron(II) systems with integer spin states (S=2), such as model systems for hemes and porphyrins.[82] EPR signals from iron centers with integer spin states are known to have low intensities (even though the spin concentration is high) and are therefore sometimes very difficult to observe. As shown in Paper V, the **F** signal's intensity drastically increased upon dilution of the Fe-OMC in a diamagnetic matrix (visible in Figure 28). If the **F** signal originates from an iron center with integer spin (S=2), the dilution method seems to be a very useful method for detection of this type of signals. The observation of the **F** signal and its possible origin as an iron(II) species is interesting because it is in agreement with the previously

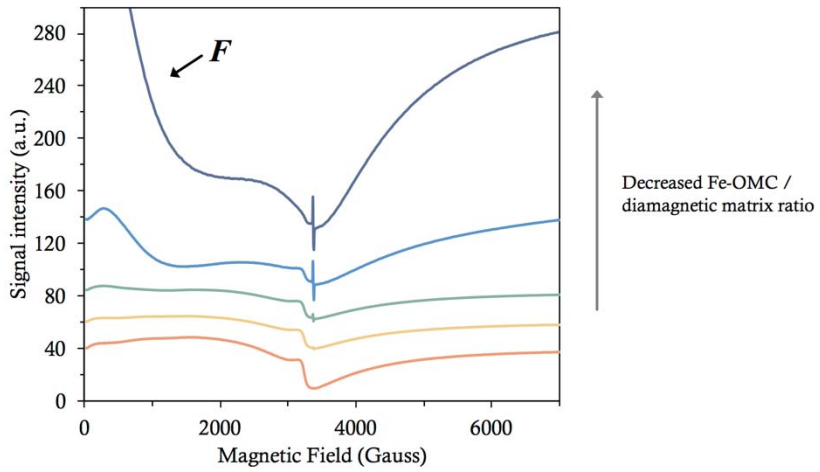

Figure 28. EPR spectra collected at 295K in air of a ball milled Fe-OMC catalyst, diluted in OM-SiO_2, with decreasing Fe-OMC/OM-SiO_2 ratio.

identified active sites in Fe-N/C catalysts; the N-$Fe^{II}N_{2+2}$/C in high spin (S=2).[57] The best way to really assign the origin of the **F** signal would be in a study combining both EPR and Mössbauer spectroscopy.

The other interesting signals which may have a relation to the active sites in the Fe-OMC catalysts are the ***R***, ***R2*** and ***O*** signals. All of the signals are highly influenced by the presence/absence of molecular oxygen and according to Paper V, it is likely that the signals are related to each other and perhaps originate from the same paramagnetic species. Two hypotheses will now be presented regarding the ***R***, ***R2*** and ***O*** signals. The first hypothesis is that the ***R*** and ***R2*** signals originate from the same species whereas the ***O*** signal originates from a superoxide radical. The g-values for the ***R*** and ***R2*** signals are typical for an axial iron(III) intermediate spin (S=3/2) where the resonance from the |+1/2>, |–1/2> transition dominates the spectrum.[85-88] This can be visualized in a rhombogram, as shown in Figure 29, [64, 89] which is useful in the interpretation of the EPR spectra. For spin systems where S >1/2, an axial (D) and a rhombic (E/D) term in zero-field splitting parameters will contribute to the spin Hamiltonian (Equation 5.2). In the rhombogram, D and E/D parameterize the axial and rhombic symmetry, respectively, where the rhombic parameter is ranging between 0≤E/D≤1/3. The second hypothesis is that the ***R*** signal originates from a rhombic iron(III) high spin (S=5/2) species where the resonance from the |+3/2>, |–3/2> transition dominates the spectrum as visible in Figure 29.[64, 87] The **R2** and ***O*** signals, in this case, originate from the same oxygen radical.[90]

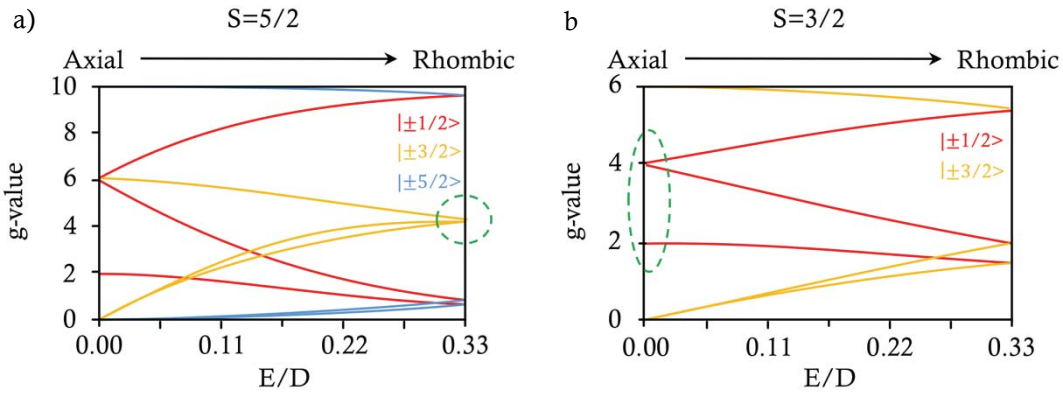

Figure 29. The principal g values for transitions |±1/2 (red), |±3/2 (yellow) and |±5/2 (blue) in spin systems (a) S=5/2 and (b) S = 3/2 as a function of the E/D term.

Irrespective of whether or not the ***R***, ***R2*** and the ***O*** signals originate from an axial or a rhombic iron species, the species (with oxidation state III, binding to an oxygen) could be related to the previously observed (N-$Fe^{III}N_4$)-O_2/C species. This iron species was previously interpreted as inactive.[57] For the iron(III)-O_2 species presented in Paper V, however, we cannot conclude if the species has oxygen reduction activity or not. It might be that the iron(III)-O_2 species is the oxidized form of an active iron(II) species (such as N-$Fe^{II}N_{2+2}$/C).

6.6.6 EPR on Fe-OMC catalysts – future outlook

In Paper V we showed that EPR spectroscopy has great potential for studying Fe-OMCs and probably also other Fe-N/C catalysts. However, much more information can most likely be extracted from the EPR-data using computer simulations, which are necessary for quantitative

interpretation of the data. Curve fitting of the EPR spectra would be helpful to confirm the already identified signals but also to identify new ones. A number of external factors were shown to influence the EPR signal and these factors could possibly be tuned further to gain even more information.

Several additional experiments would be interesting to do, such as: *i)* decrease the measurement temperature to around 2-5 K to increase the intensity of some of the signals and extract more information, *ii)* increase the measurement temperature to 353K (80°C), to study the Fe-OMC catalysts in the working temperature of the fuel cell, *iii)* EPR *in-situ* studies of the catalyst in a fuel cell, *iv)* possibly visualize more of the O_2-iron(III) species by increasing the oxygen concentration and oxiding the iron(II) species, *v)* preparation of a Fe-OMC catalyst synthesized from Fe^{57} enriched iron chloride. The EPR signals of Fe-OMCs prepared with Fe^{57} or Fe^{56}, respectively, most likely have different EPR-spectra. The Fe^{57} nuclei has a spin abundance of ½ which will split the EPR-signal of the neighboring unpaired electrons due to hyperfine interactions. The Fe^{56} nuclei however, has zero spin abundance and does not split the signals. A Fe-OMC prepared from Fe^{57} enriched iron salt could also be analyzed by Mössbauer spectroscopy, which would be a valuable complement to the EPR-results.

7. The carbon support – to achieve active catalysts

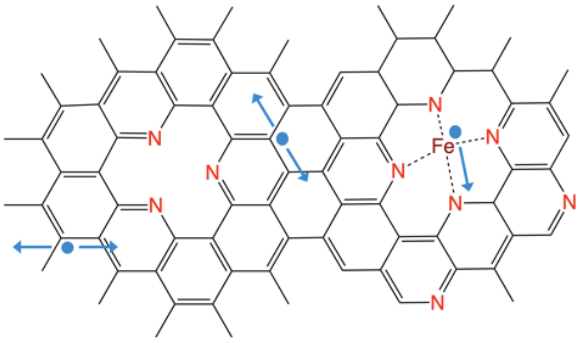

Until now the focus in the thesis has been on understanding the active sites in our catalysts. However, material related properties of the carbon matrix should not be forgotten. The active sites require a suitable support material in order to perform as efficiently as possible. The better the active sites are connected to the carbon matrix in regard to electron transfer capabilities, the more efficient the catalyst. Therefore, this chapter is dedicated to aspects related to the carbon support in the catalyst. This chapter also brings up problems with the catalyst synthesis approach and how to modify it.

7.1 Influence of furfurylalcohol in the precursor mixture on the carbon formation

In Paper II, we wanted to improve the properties of the carbon matrix of our OMCs regarding pore structure, surface properties and conductivity to increase the mass transport and decrease electrical resistivity in the catalysts. This was done by adding furfurylalcohol to the typical synthesis of Fe-OMCs made of furfurylamine. The hypothesis was to form a two-component system; where the furfurylamine and the $FeCl_3$ form chelates resulting in active catalytic sites and the furfurylalcohol incorporates these active sites in an efficient carbon matrix. Carbon and electrochemical properties of the catalysts were thereafter characterized to understand how the carbon structure influences the catalytic performance.

From characterization by nitrogen sorption, Raman, XRD and SAXS, it became clear that the carbon properties of the Fe-OMC catalyst varied dependent on if furfurylalcohol was added to the synthesis or not. The variations can be explained by different crosslinking mechanisms of the two carbon precursors, which will influence the type and number of defects in the carbon's conjugated system. The conjugated system, which determines the carbon's conductivity, can be influenced/disturbed by defects in the structure involving; grain boundaries/edges, in-plane substituted heteroatoms, vacancies, and/or sp^3-hybridization. Furfurylalcohol, with its high reactive nature, allows for effective precursor polymerization in three dimensions, resulting in a highly meso-ordered cubic structure with high surface area. Coexistence of sp^2- and sp^3-carbon hybridization is necessary to reach such high order and surface area, and which is facilitated by addition of furfurylalcohol. A larger surface area of the catalyst results in a higher number of surface-exposed active sites. The carbon of the Fe-OMCs prepared with the furfurylalcohol addition, also obtained an increased conductivity. The conjugated system appears more complete and facilitates the electron transfer in the material. This explains the lower resistivity in these catalysts and the higher ORR-activity as shown in Figure 30.

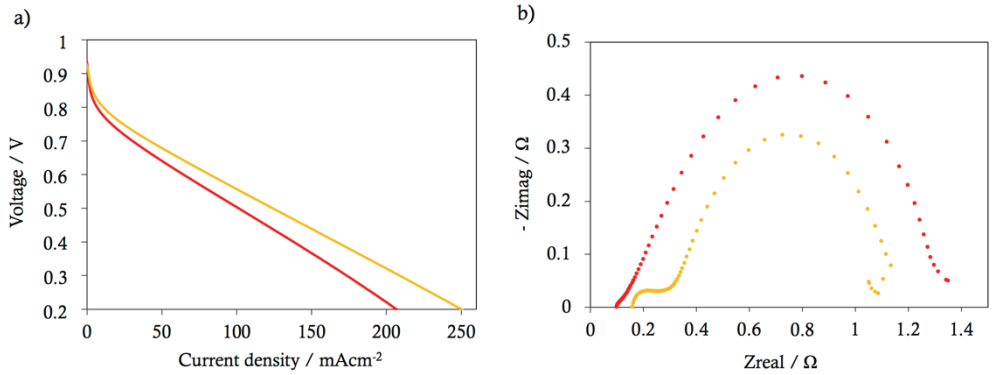

Figure 30. Fuel cell polarization curves (a) and Nyquist plot measured at 0.7 V (b) of $FuNH_2$-Fe (red) and $FuNH_2$-Fe-FuOH (yellow).

7.2 Influence of iron precursor hydration state on the carbon formation

In Paper I, three parameters; *i)* hydration state of $FeCl_3$, *ii)* precursor aging time and *iii)* iron to N/C-precursor ratio, were found to influence the complex formation and the activity of the Fe-OMCs. The same parameters were also found to affect the impregnation process and the crosslinking possibilities of the precursor mixtures and consequently also the pore and surface properties of the catalysts. Iron chloride catalyzes the crosslinking reaction of the furfurylamine and therefore a high iron content increased the precursor's ability to cross link which is favorable to reach high surface area. A too high iron content however, increased the viscosity of the precursor mixture which resulted in a poor impregnation and low surface area. By the use of the hydrated $FeCl_3$ it was possible to make $FeCl_3$-furfurylamine precursor mixtures with much higher iron/furfurylamine molar ratio which was favorable for increasing the activity of the catalysts.

7.3 Improved activity by milder route of preparation

A requirement in developing Fe-OMC catalysts is to achieve a low degree of complexity of the catalyst preparation in order to further reduce cost. One crucial and complex step in the synthesis is the removal of the silica template as shown in Figure 31. It is after the etch the catalysts obtain their high specific surface area and porous structure. When designing the etch method it is important to consider an etch chemical which dissolves the silica but does not affect or dissolve the active iron chelates. In principle, the silica can be removed by either etching in acidic HF or alkaline KOH or NaOH solutions. In previous work made on Fe-OMCs only HF etch has been used to remove the silica. HF efficiently dissolves the silica and keeps the chelated transition metal ions intact and electrocatalytically active after the etching. Unfortunately, HF is an unpleasantly hazardous and toxic acid and the use of it should be avoided. Therefore, in Paper III we tried an alternative milder etch method based on alkaline NaOH and applied it on the synthesis of Fe-OMCs. The effect on the carbon properties and the catalytic performance was studied in comparison to the HF method. We found that an etch method based on NaOH, efficiently removes the silica template and increases the catalytic activity of the Fe-OMC catalyst compared to when using the HF etch as shown in the fuel cell data in Figure 32. To gain more insight about why the two etch methods give rise to such different fuel cell results in the Fe-OMCs, we applied EPR spectroscopy and this will be discussed in the next section.

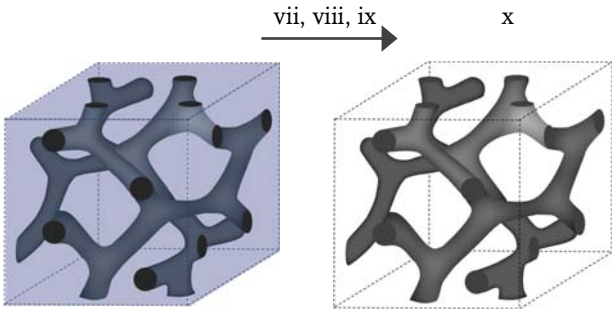

Figure 31. Schematic diagram of the last steps in the synthesis procedure: (vii) silica template removal by HF or NaOH, (viii) sulfuric acid treatment, (ix) second pyrolysis treatment (950°C for 2 h in nitrogen), and (x) the final catalyst.

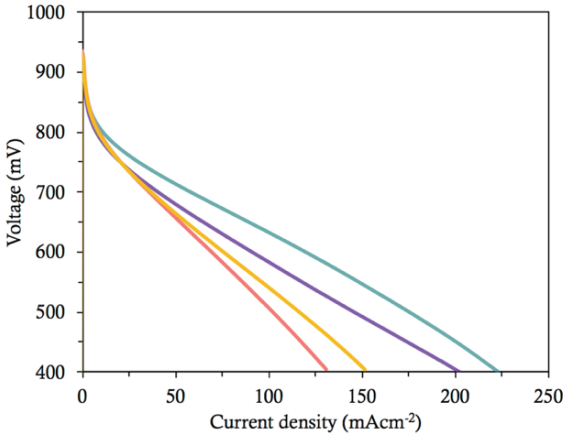

Figure 32. Fuel cell polarization curves of $FuNH_2$-Fe-HF (pink), $FuNH_2$-Fe-FuOH-HF (yellow), $FuNH_2$-Fe-NaOH (purple) and $FuNH_2$-Fe-FuOH-NaOH (turquoise).

7.4 EPR to study carbon properties of Fe-OMCs

EPR does not only give information about the iron species in the Fe-OMCs, it can also give important information about the electronic structure of the supporting carbon matrix. One EPR signal, the ***C*** signal, found in Fe-OMC samples both in Paper III and V, are believed to originate from delocalized electrons in the conductive carbon support. The ***C*** signal was particularly visible in the EPR spectra of the Fe-OMCs treated with the NaOH etch as shown in Figure 33. In the EPR spectra in the left figure, a NaOH treated Fe-OMC (turquoise trace) is compared to a HF treated Fe-OMC (yellow trace) from Paper III, and in the right figure the dark blue trace shows EPR spectra of another NaOH treated Fe-OMC catalyst. The ***C*** signal, between 2000–4000 Gauss, seems to be dominating the spectra but is probably superimposed with other signals. Interestingly, the ***C*** signal was also found in the EPR spectra of another Fe-OMC (Fe-FC60) sample prepared in a previous study.[91] This Fe-OMC sample (treated with HF) was identified to have highly graphitic properties due to presence of multi walled carbon tubes formed during the synthesis. All the Fe-OMCs with the identified ***C*** signal showed increased catalytic performance at higher current densities (as visible in Figure 32, turquoise) which could be an indication of higher conductivity in the carbon structure.

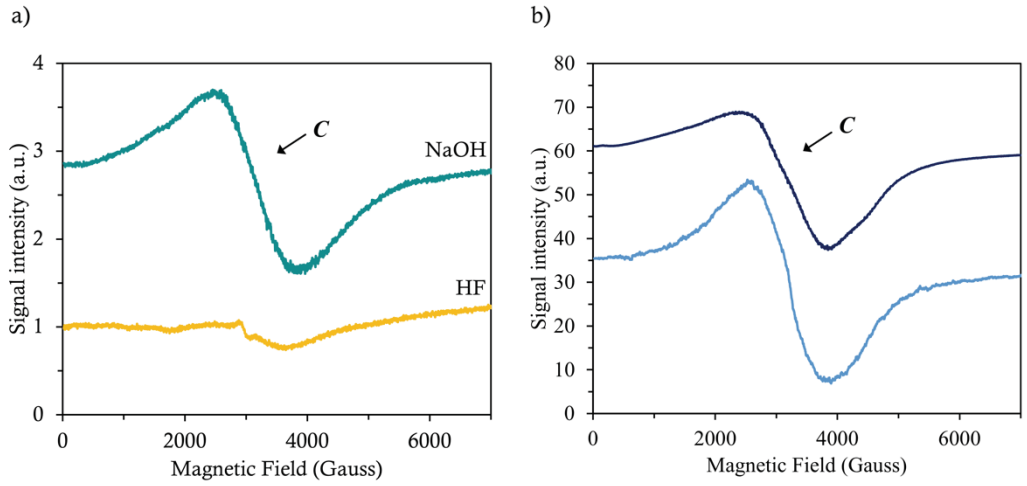

Figure 33. EPR spectra of (a) FuNH2-Fe-FuOH-NaOH (turquoise), FuNH2-Fe-FuOH-HF (yellow), and (b) NaOH treated Fe-OMC sample (dark blue), HF treated Fe-FC60 (blue) collected at 295K in air.

7.5 Improved activity by optimizing the pyrolysis temperature

In a previous study it was investigated how the Fe-OMC's catalytic activity varied with pyrolysis temperature.[10] The activity was increased with increasing pyrolysis temperature from (700-1100°C) up to a certain point (1200°C) where the activity was drastically reduced. It is known that the formation of active sites in iron-nitrogen based ORR-catalysts is favored at pyrolysis temperatures between 800-950°C.[92] Below and above that pyrolysis temperature range, the active sites have likely not been formed or started to decompose, respectively. However, it is also known that the conductivity in many carbon materials is improved with increasing pyrolysis temperature.[93-94] In Paper V we look into this further and studied both the iron species and the electronic structure of the carbon simultaneously by EPR spectroscopy. As shown in Figure 34, a large variation between the Fe-OMC samples (synthesized with different pyrolysis temperatures) can be observed in the EPR spectra. This suggests that a transformation of the iron local structure and/or carbon structure occurs when the pyrolysis temperature is increased from 700°C to 1200°C.

From Paper V we found that the increased catalytic activity in the Fe-OMC-1100 sample can be due to improved carbon support properties, in combination with active sites. It is possible that the samples Fe-OMC-700 to Fe-OMC-950 consist of a similar type of active sites (and perhaps at a higher concentration) as in Fe-OMC-1100, but are lacking in activity because of poorer carbon matrix properties. In the ideal system, a large number of active sites are interconnected in a highly conducting carbon matrix, and the delocalized electrons can move freely between the active sites and the carbon matrix as shown in Figure 35. For the Fe-OMCs, as they have been synthesized in this thesis, it seems to be a trade-off between having many active sites and having a highly conductive carbon matrix, both of which are necessary in the right proportions to reach the highest catalytic activity. Even though the Fe-OMC-1100 sample possibly contains fewer active sites compared to the Fe-OMC-950 sample, the higher conductivity of the Fe-OMC-1100 sample seems to more than compensate for that, resulting in a more catalytically active catalyst. For future studies it would be interesting to synthesize new Fe-OMC catalysts and vary the pyrolysis temperature between 950 and 1200 °C to find the optimum temperature to reach the best catalytic

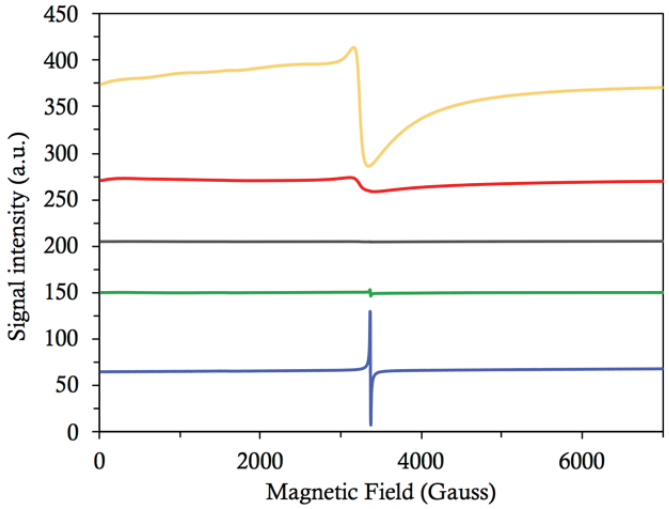

Figure 34. EPR spectra of ball milled Fe-OMC catalysts pyrolyzed at 700°C (blue), 800°C (green), 950°C (black), 1100°C (red) and 1200°C (yellow) collected at 295K in air.

activity. Additionally, it would be interesting to mix one of the samples pyrolyzed at lower temperatures (700-950 °C) with a highly conductive carbon material. If these samples contain high concentration of active sites the additional conductive carbon support may serve the active sites more efficiently to reach higher catalytic activity. In that way the optimum pyrolysis temperature (to create active sites with the highest activity) can be identified.

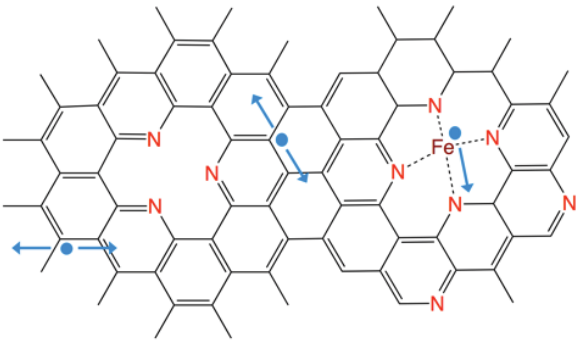

Figure 35. 2D illustration of the carbon structure and the delocalized electron (blue dots) mobility between the active sites and the carbon matrix.

8. Conclusions

One aim of this thesis was to tune and simplify the method of preparing iron-nitrogen chelating ordered mesoporous carbon catalysts with improved catalytic activity. The focus has been put on developing a deeper understanding of the operational mechanism behind the active site in the catalysts, and explore analytical methods to study it. Furthermore, modifications of the synthesis method were made to achieve more efficient carbon support for the catalysts. The following valuable knowledge and improvements regarding the catalysts were gained.

(i) From the obtained fuel cell and EPR results, the previous theory was strengthened, that nitrogen is involved in the formation of active sites in the Fe-OMC catalysts.

(ii) Parameters such as hydration state of the iron salt, precursor aging time, and iron to N/C-precursor ratio, were shown to influence both the iron-nitrogen interactions/complex formation and the catalytic activity of the Fe-OMC catalysts.

(iii) Correlations between the initial iron-nitrogen interactions in the precursor and the activity in the final catalyst were made and may in the future allow for screening potential metal/N/C-precursor combinations in early stage of the synthesis.

(iv) NMR was found useful as a method to study the precursor mixtures and identify iron-nitrogen interactions.

(v) Different iron salts in the synthesis of Fe-OMCs influence the *type* of iron species formed. Higher solubility of the iron salt in the N/C precursor does not necessarily increase the iron loading of the Fe-OMC and a high iron loading does not necessarily indicate a large concentration of active sites.

(vi) EPR spectroscopy can contribute with substantial information regarding the iron species, oxygen radicals, and delocalized electrons in the Fe-OMCs. Essential information about the iron species such as type, oxidation state, geometry and interaction with oxygen can relatively simply be identified. Proper sample preparation is necessary for most Fe-OMC catalysts to obtain high quality EPR data.

(vii) By addition of furfurylalcohol to the precursor composition the carbon matrix properties were improved.

(viii) The unpleasant HF etch was found to be replaceable by an NaOH etch and an increased catalytic activity was observed.

(ix) Fe-OMC with high conductivity (in combination with active sites) seems to be important to reach highly active catalysts. There appears to be a trade-off between having many active sites and having a highly conductive carbon matrix, both of which are necessary in the right proportions to reach the highest catalytic activity.

With these results, we achieved small steps forward towards a more efficient catalyst. Even though the steps are small, each step is important for understanding and optimizing the catalyst. Many parameters influence the catalyst performance and each small step adds up and hopefully a great improvement will be reached at the end. The more knowledge we gain about our catalyst, the easier it will become to tune the catalysts to be as active, efficient and cheap as possible.

9. Acknowledgements

First of all, Chalmers Area of Advance Nanoscience and Nanotechnology is gratefully acknowledged for funding this project. Part of the work has also been supported by the Swedish Energy Agency (Energimyndigheten) through project 38340-1.

Then I would like to thank the following people:

Min handledare Anders Palmqvist. Du är en handledare med höga visioner, något jag uppskattar mycket. Jag känner verkligen att du litar på min förmåga och att du lyssnar på mina idéer, samtidigt som du alltid kommer med värdefulla åsikter och tankar som gör allt mycket bättre. Det är väldigt lärorikt att jobba med dig. Du är en väldigt omtänksam person. Tack!

My former colleague, co-author, and friend Johanna Dombrovskis for all help and support in the fuel cell lab. I am very happy that we were able to write an article together and it was very nice to have you as a close colleague. My colleges, co-authors and friends Sam and Walter. I enjoyed doing a study with you two, it is much more fun to do something together than alone. And Walter thank you for all your help in fuel cell lab.

Min examinator Hanna Härelind. Jag kunde inte haft en bättre examinator! Tack för peppning och stöd, du visar verkligen att du finns där och vill hjälpa till. Lars Nordstierna för all hjälp och engagemang i och med mina NMR mätningar, uppskattar dig även mycket som vän. Anna Martinelli för all hjälp och engagemang i och med mina Raman mätningar. Frida, Ann och Kristina för hjälp med alla viktiga papper och Anne and Romain för all praktisk hjälp i labbet.

People at University of California Santa Barbara: Brad Chmelka, Songi Han, Ilia Kaminker, Jaya Nolt, Timothy Keller, Niels Zussblatt for guidance and valuable inputs when I visited University of California, Santa Barbara for EPR-measurements.

My research group and former group! Sanna, Milene, Giulio, Gunnar, Yifei, Joakim, Andrey, Tim, Ralph, Björn, Florian you are all great! TYK and KCK, I am very happy to have so many beautiful and fun people around. Especially thanks to Ting, Mats, Saba, Simon, Anand, Astrid and Anna.

Mina fina vänner, Yasmin, Johanna, Amila, Sara, Johanna, Erica, Kajsa, Sina, Malin, Hanna utanför den här världen som förgyller vardagen!

Min familj, Mamma, Pappa, Björn, Maëva, Sólveig, Adélie, Cecilia och Calle som är dom bästa och som alltid uppmuntrar mig och stöttar mig i allt jag gör. Min släkt och speciellt tack till Kerstin, som tagit dig rollen som min mentor, jag är väldigt tacksam för dina uppmuntrande och klocka tankar. Geirs familj som är världens snällaste och mest stöttande och som tar med mig på massa roliga spännande resor! Min älskade Geir. Som har stått ut med mig senaste året. Tack för att du ställer kluriga frågor som gör att man får tänka till och tack för att du tror på mig.

10. Abbreviations

EPR - Electron Paramagnetic Resonance
EXAFS - Extended X-Ray Absorption Fine Structure
Fe-OMC – Iron-Chelating Ordered Mesoporous Carbon
HOR – Hydrogen Oxidation Reaction
NMR - Nuclear Magnetic Resonance
PEMFC – Proton Exchange Membrane Fuel Cell
OMC – Ordered Mesoporous Carbon
ORR – Oxygen Reduction Reaction
SAXS – Small angle X-ray scattering
TM-OMC – Transition Metal-Chelating Ordered Mesoporous Carbon
XAFS - X-ray Absorption Fine Structure
XRD – X-ray Diffraction

11. References

1. Sachs, J. D., *The Age of Sustainable Development*. Columbia University Press: 2015.
2. United Nations. *Transforming our world: the 2030 Agenda for Sustainable Development*; 2015.
3. Wang, M. Y.; Wang, Z.; Gong, X. Z.; Guo, Z. C., The intensification technologies to water electrolysis for hydrogen production - A review. *Renew Sust Energ Rev* **2014,** *29*, 573-588.
4. Chi, J.; Yu, H., Water electrolysis based on renewable energy for hydrogen production. *Chinese Journal of Catalysis* **2018,** *39* (3), 390-394.
5. Maeda, K.; Domen, K., Photocatalytic Water Splitting: Recent Progress and Future Challenges. *J Phys Chem Lett* **2010,** *1* (18), 2655-2661.
6. Råde, I. Requirement and Availability of Scarce Metals for Fuel-Cell and Battery Electric Vehicles. Chalmers University of Technology, Gothenburg, 2001.
7. James, B. D.; Huya-Kouadio, J. M.; Houchins, C.; DeSantis, D. A. *Mass Production Cost Estimation of Direct H2 PEM Fuel Cell Systems for Transportation Applications: 2016 Update*; Strategic Analysis Inc: 2016.
8. Chen, Z.; Dodelet, J.-P.; Dodelet, J. Z., *Non-Noble Metal Fuel Cell Catalysts*. Wiley-VCH Verlag GmbH & Co. KGaA: Weinheim, Germany, 2014.
9. Dombrovskis, J. K.; Jeong, H. Y.; Fossum, K.; Terasaki, O.; Palmqvist, A. E. C., Transition Metal Ion-Chelating Ordered Mesoporous Carbons as Noble Metal-Free Fuel Cell Catalysts. *Chem Mater* **2013,** *25* (6), 856-861.
10. Dombrovskis, J. K.; Palmqvist, A. E. C., The Active Site Structure of Transition Metal Ion-Chelating Ordered Mesoporous Carbon Fuel Cell Catalysts. *Fuel Cells* **2016,** *16* (1), 23-31.
11. Dombrovskis, J. K. Functionalized mesoporous carbons as non-precious metal fuel cell catalysts. Chalmers University of Technology, Gothenburg, 2016.
12. Davy, H., An Account of Some Galvanic Combinations, Formed by the Arrangement of Single Metallic Plates and Fluids, Analogous to the New Galvanic Apparatus of Mr. Volta. *Philosophical Transactions of the Royal Society of London* **1801,** *91*, 397-402.
13. Grove, W. R., XXIV. On voltaic series and the combination of gases by platinum. *Philosophical Magazine Series 3* **1839,** *14* (86-87), 127-130.
14. Hydrogen Cars Now. 1966 GM Electrovan. http://www.hydrogencarsnow.com/index.php/gm-electrovan/ (accessed 18 April).
15. Curtin, S.; Gangi, J. *Fuel Cell Technologies Market Report 2015*; Fuel Cell and Hydrogen Energy Association: Washington, D.C., 2015.
16. Larminie, J.; Dicks, A., Introduction. In *Fuel Cell Systems Explained*, John Wiley & Sons, Ltd,. 2013; pp 1-24.
17. Hirschenhofer, J. H.; Stauffer, D. B.; Engleman, R. R.; Klett, M. G., *Fuel Cell Handbook*. 4th ed.; 1998.
18. Ruether, J.; Ramezan, M.; Grol, E. *Life-cycle analysis of greenhouse gas emissions for hydrogen fuel production in the United States from LNG and Coal*; DOE/NETL-2006/1227 Report, 2005.
19. Collodi, G., Hydrogen Production via Steam Reforming with CO(2) Capture. In *4th International Conference on Safety & Environment in Process Industry*, Buratti, S. s., Ed. Chemical Engineering Transactions: 2010; Vol. 19.
20. Godula-Jopek, A.; Jehle, W.; Wellnitz, J. r., *Hydrogen storage technologies : new materials, transport, and infrastructure*. Wiley-VCH: Weinheim, 2012; p ix, 254 p.
21. Larminie, J.; Dicks, A., Efficiency and Open Circuit Voltage. In *Fuel Cell Systems Explained*, John Wiley & Sons, Ltd,. 2013; pp 25-43.
22. Williams, M., *Fuel Cell Handbook*. 7th ed.; US Deparment of Energy: 2004.
23. Pletcher, D., *A first course in electrode processes*. The Royal Society of Chemistry: Cambridge, U.K., 2009.
24. Larminie, J.; Dicks, A., Operational Fuel Cell Voltages. In *Fuel Cell Systems Explained*, John Wiley & Sons, Ltd,. 2013; pp 45-66.

25. Marcinkoski, J.; Spendelow, J.; Wilson, A.; Papageorgopoulos, D. *Fuel Cell System Cost - 2015*; DOE Hydrogen and Fuel Cells Program Record, 2015.
26. Wang, B., Recent development of non-platinum catalysts for oxygen reduction reaction. *J Power Sources* **2005,** *152* (1), 1-15.
27. Bron, M., Electrocatalysts for Acid Proton Exchange Membrane (PEM) Fuel Cells – an Overview. In *Non-Noble Metal Fuel Cell Catalysts*, Wiley-VCH Verlag GmbH & Co. KGaA: 2014; pp 1-28.
28. Lee, J. W.; Popov, B. N., Ruthenium-based electrocatalysts for oxygen reduction reaction - a review. *J Solid State Electr* **2007,** *11* (10), 1355-1364.
29. Zhang, L.; Zhang, J. J.; Wilkinson, D. P.; Wang, H. J., Progress in preparation of non-noble electrocatalysts for PEM fuel cell reactions. *J Power Sources* **2006,** *156* (2), 171-182.
30. Alonso-Vante, N.; Bogdanoff, P.; Tributsch, H., On the origin of the selectivity of oxygen reduction of ruthenium-containing electrocatalysts in methanol-containing electrolyte. *J Catal* **2000,** *190* (2), 240-246.
31. Schmidt, T. J.; Paulus, U. A.; Gasteiger, H. A.; Alonso-Vante, N.; Behm, R. J., Oxygen reduction on Ru1.92Mo0.08SeO4, Ru/carbon, and Pt/carbon in pure and methanol-containing electrolytes. *J Electrochem Soc* **2000,** *147* (7), 2620-2624.
32. Gong, K. P.; Du, F.; Xia, Z. H.; Durstock, M.; Dai, L. M., Nitrogen-Doped Carbon Nanotube Arrays with High Electrocatalytic Activity for Oxygen Reduction. *Science* **2009,** *323* (5915), 760-764.
33. Nagaiah, T. C.; Kundu, S.; Bron, M.; Muhler, M.; Schuhmann, W., Nitrogen-doped carbon nanotubes as a cathode catalyst for the oxygen reduction reaction in alkaline medium. *Electrochemistry Communications* **2010,** *12* (3), 338-341.
34. Biddinger, E. J.; von Deak, D.; Ozkan, U. S., Nitrogen-Containing Carbon Nanostructures as Oxygen-Reduction Catalysts. *Top Catal* **2009,** *52* (11), 1566-1574.
35. Jasinski, R., New Fuel Cell Cathode Catalyst. *Nature* **1964,** *201* (492), 1212-1213.
36. Jahnke, H.; Schönborn, M.; Zimmermann, G. In *Organic dyestuffs as catalysts for fuel cells*, Berlin, Heidelberg, Springer Berlin Heidelberg: Berlin, Heidelberg, 1976; pp 133-181.
37. Li, Z. P.; Liu, B. H., The use of macrocyclic compounds as electrocatalysts in fuel cells. *J Appl Electrochem* **2010,** *40* (3), 475-483.
38. Wiesener, K., N-4-Chelates as Electrocatalyst for Cathodic Oxygen Reduction. *Electrochim Acta* **1986,** *31* (8), 1073-1078.
39. Scherson, D. A.; Gupta, S. L.; Fierro, C.; Yeager, E. B.; Kordesch, M. E.; Eldridge, J.; Hoffman, R. W.; Blue, J., Cobalt tetramethoxyphenyl porphyrin—emission Mossbauer spectroscopy and O2 reduction electrochemical studies. *Electrochim Acta* **1983,** *28* (9), 1205-1209.
40. Yeager, E., Dioxygen electrocatalysis: mechanisms in relation to catalyst structure. *Journal of Molecular Catalysis* **1986,** *38* (1), 5-25.
41. van Veen, J. A. R.; Colijn, H. A.; van Baar, J. F., On the effect of a heat treatment on the structure of carbon-supported metalloporphyrins and phthalocyanines. *Electrochim Acta* **1988,** *33* (6), 801-804.
42. Franke, R.; Ohms, D.; Wiesener, K., Investigation of the influence of thermal treatment on the properties of carbon materials modified by N4-chelates for the reduction of oxygen in acidic media. *Journal of Electroanalytical Chemistry and Interfacial Electrochemistry* **1989,** *260* (1), 63-73.
43. Bashyam, R.; Zelenay, P., A class of non-precious metal composite catalysts for fuel cells. *Nature* **2006,** *443* (7107), 63-66.
44. Lefevre, M.; Proietti, E.; Jaouen, F.; Dodelet, J. P., Iron-Based Catalysts with Improved Oxygen Reduction Activity in Polymer Electrolyte Fuel Cells. *Science* **2009,** *324* (5923), 71-74.
45. Proietti, E.; Jaouen, F.; Lefevre, M.; Larouche, N.; Tian, J.; Herranz, J.; Dodelet, J. P., Iron-based cathode catalyst with enhanced power density in polymer electrolyte membrane fuel cells. *Nat Commun* **2011,** *2*.
46. Wu, G.; More, K. L.; Johnston, C. M.; Zelenay, P., High-Performance Electrocatalysts for Oxygen Reduction Derived from Polyaniline, Iron, and Cobalt. *Science* **2011,** *332* (6028), 443-447.

47. Wang, Y. C.; Lai, Y. J.; Song, L.; Zhou, Z. Y.; Liu, J. G.; Wang, Q.; Yang, X. D.; Chen, C.; Shi, W.; Zheng, Y. P.; Rauf, M.; Sun, S. G., S-Doping of an Fe/N/C ORR Catalyst for Polymer Electrolyte Membrane Fuel Cells with High Power Density. *Angew Chem Int Edit* **2015,** *54* (34), 9907-9910.
48. Shui, J. L.; Chen, C.; Grabstanowicz, L.; Zhao, D.; Liu, D. J., Highly efficient nonprecious metal catalyst prepared with metal-organic framework in a continuous carbon nanofibrous network. *P Natl Acad Sci USA* **2015,** *112* (34), 10629-10634.
49. Tian, J.; Morozan, A.; Sougrati, M. T.; Lefevre, M.; Chenitz, R.; Dodelet, J. P.; Jones, D.; Jaouen, F., Optimized Synthesis of Fe/N/C Cathode Catalysts for PEM Fuel Cells: A Matter of Iron-Ligand Coordination Strength. *Angew Chem Int Edit* **2013,** *52* (27), 6867-6870.
50. Tributsch, H.; Koslowski, U. I.; Dorbandt, I., Experimental and theoretical modeling of Fe-, Co-, Cu-, Mn-based electrocatalysts for oxygen reduction. *Electrochim Acta* **2008,** *53* (5), 2198-2209.
51. Ziegelbauer, J. M.; Olson, T. S.; Pylypenko, S.; Alamgir, F.; Jaye, C.; Atanassov, P.; Mukerjee, S., Direct spectroscopic observation of the structural origin of peroxide generation from co-based pyrolyzed porphyrins for ORR applications. *J Phys Chem C* **2008,** *112* (24), 8839-8849.
52. Lalande, G.; Cote, R.; Guay, D.; Dodelet, J. P.; Weng, L. T.; Bertrand, P., Is nitrogen important in the formulation of Fe-based catalysts for oxygen reduction in solid polymer fuel cells? *Electrochim Acta* **1997,** *42* (9), 1379-1388.
53. Dodelet, J.-P., Oxygen Reduction in PEM Fuel Cell Conditions: Heat-Treated Non-Precious Metal-N4 Macrocycles and Beyond. In *N4-Macrocyclic Metal Complexes*, Zagal, J. H.; Bedioui, F.; Dodelet, J.-P., Eds. Springer New York: New York, NY, 2006; pp 83-147.
54. Bezerra, C. W. B.; Zhang, L.; Lee, K. C.; Liu, H. S.; Marques, A. L. B.; Marques, E. P.; Wang, H. J.; Zhang, J. J., A review of Fe-N/C and Co-N/C catalysts for the oxygen reduction reaction. *Electrochim Acta* **2008,** *53* (15), 4937-4951.
55. Lefevre, M.; Dodelet, J. P., Recent Advances in Non-precious Metal Electrocatalysts for Oxygen Reduction in PEM Fuel Cells. *Tutorials on Electrocatalysis in Low Temperature Fuel Cells* **2012,** *45* (2), 35-44.
56. Li, X. G.; Popov, B. N.; Kawahara, T.; Yanagi, H., Recent Advances in Non-Precious Metal Catalysts for Oxygen Reduction Reaction in Fuel Cells. *Polymer Electrolyte Fuel Cells 10, Pts 1 and 2* **2010,** *33* (1), 1769-1776.
57. Kramm, U. I.; Herranz, J.; Larouche, N.; Arruda, T. M.; Lefevre, M.; Jaouen, F.; Bogdanoff, P.; Fiechter, S.; Abs-Wurmbach, I.; Mukerjee, S.; Dodelet, J. P., Structure of the catalytic sites in Fe/N/C-catalysts for O2-reduction in PEM fuel cells. *Phys Chem Chem Phys* **2012,** *14* (33), 11673-88.
58. Jaouen, F.; Goellner, V.; Lefevre, M.; Herranz, J.; Proietti, E.; Dodelet, J. P., Oxygen reduction activities compared in rotating-disk electrode and proton exchange membrane fuel cells for highly active Fe-N-C catalysts. *Electrochim Acta* **2013,** *87*, 619-628.
59. Kleitz, F.; Hei Choi, S.; Ryoo, R., Cubic Ia3d large mesoporous silica: synthesis and replication to platinum nanowires, carbon nanorods and carbon nanotubes. *Chemical Communications* **2003,** (17), 2136-2137.
60. Dombrovskis, J. K.; Palmqvist, A. E. C., Recent Progress in Synthesis, Characterization and Evaluation of Non-Precious Metal Catalysts for the Oxygen Reduction Reaction. *Fuel Cells* **2016,** *16* (1), 4-22.
61. Keeler, J., *Understanding NMR Spectroscopy*. Wiley: 2010.
62. Bertini, I.; Luchinat, C.; Parigi, G. Chapter 1 - Introduction. In *Current Methods in Inorganic Chemistry*. Elsevier: 2001; Vol. 2, pp 1-28.
63. Varnell, J. A.; Tse, E. C. M.; Schulz, C. E.; Fister, T. T.; Haasch, R. T.; Timoshenko, J.; Frenkel, A. I.; Gewirth, A. A., Identification of carbon-encapsulated iron nanoparticles as active species in non-precious metal oxygen reduction catalysts. *Nat Commun* **2016,** *7*.
64. Petasis, D. T.; Hendrich, M. P., Quantitative interpretation of EPR spectroscopy with applications for iron-sulfur proteins In *Iron-Sulfur Clusters in Chemistry and Biology*, Rouault, T. A., Ed. 2014; pp 21-48.

65. Eaton, G. R.; Eaton, S. S.; Barr, D. P.; Weber, R. T., *Quantitative EPR*. SpringerWienNewYork: Germany, 2010.
66. Jiang, J.; Weber, R. T. *Elexsys E 500 User's Manual Basic Operations*; EPR Division Bruker BioSpin Corporation: USA, 2001.
67. Brunauer, S.; Emmett, P. H.; Teller, E., Adsorption of gases in multimolecular layers. *J Am Chem Soc* **1938,** *60*, 309-319.
68. Barrett, E. P.; Joyner, L. G.; Halenda, P. P., The Determination of Pore Volume and Area Distributions in Porous Substances .1. Computations from Nitrogen Isotherms. *J Am Chem Soc* **1951,** *73* (1), 373-380.
69. Joyner, L. G.; Barrett, E. P.; Skold, R., The Determination of Pore Volume and Area Distributions in Porous Substances .2. Comparison between Nitrogen Isotherm and Mercury Porosimeter Methods. *J Am Chem Soc* **1951,** *73* (7), 3155-3158.
70. Lambert, J. B.; Gronert, S.; Shurvell, H. F.; Lightner, D. A., *Organic Structural Spectroscopy*. 2nd ed.; Pearson Prentice Hall: 1998.
71. Rhodes, G., *Crystallography Made Crystal Clear*. 3rd ed.; Academic Press: 2006.
72. Glatter, O.; Kratky, O., *Small Angle X-ray Scattering*. Academic Press: 1982.
73. Dombrovskis, J. K.; Prestel, C.; Palmqvist, A. E. C., Optimization of fuel cell membrane electrode assemblies for transition metal ion-chelating ordered mesoporous carbon cathode catalysts. *Apl Mater* **2014,** *2* (12).
74. Bard, A. J., *Electrochemical Methods*. 2nd ed.; John Wiley and Sons (WIE): 2000.
75. Linberg, R.; Conover, C. D.; Shum, K. L., Hemoglobin Based Oxygen Carriers: How Much Methemoglobin is too Much? *Artificial Cells, Blood Substitutes, and Biotechnology* **1998,** *26* (2), 133-148.
76. Zhang, L., *Heme Biology*. World Scientific Publishing Company: Singapore, USA, 2011.
77. Poulos, T. L., Heme enzyme structure and function. *Chem Rev* **2014,** *114* (7), 3919-62.
78. Bezerra, C. W. B.; Zhang, L.; Liu, H.; Lee, K.; Marques, A. L. B.; Marques, E. P.; Wang, H.; Zhang, J., A review of heat-treatment effects on activity and stability of PEM fuel cell catalysts for oxygen reduction reaction. *J Power Sources* **2007,** *173* (2), 891-908.
79. Koksharov, Y. A.; Pankratov, D. A.; Gubin, S. P.; Kosobudsky, I. D.; Beltran, M.; Khodorkovsky, Y.; Tishin, A. M., Electron paramagnetic resonance of ferrite nanoparticles. *Journal of Applied Physics* **2001,** *89* (4), 2293-2298.
80. Misra, S.; Andronenko, S.; M. Reddy, K.; Hays, J.; Thurber, A.; Punnoose, A., A variable temperature Fe^{3+} electron paramagnetic resonance study of $Sn_{1-x}Fe_xO_2$ ($0.00 \leq x \leq 0.05$). *Journal of Applied Physics* **2007**; *101*, 09H120.
81. Housecroft, E. C.; Sharpe, A. G., *Inorganic Chemistry*. Pearson: 2001.
82. Hendrich, M. P.; Debrunner, P. G., Integer-Spin Electron-Paramagnetic Resonance of Iron Proteins. *Biophys J* **1989,** *56* (3), 489-506.
83. Sahraie, N. R.; Kramm, U. I.; Steinberg, J.; Zhang, Y.; Thomas, A.; Reier, T.; Paraknowitsch, J. P.; Strasser, P., Quantifying the density and utilization of active sites in non-precious metal oxygen electroreduction catalysts. *Nat Commun* **2015,** *6*, 8618.
84. Kramm, U. I.; Lefevre, M.; Larouche, N.; Schmeisser, D.; Dodelet, J. P., Correlations between Mass Activity and Physicochemical Properties of Fe/N/C Catalysts for the ORR in PEM Fuel Cell via Fe-57 Mossbauer Spectroscopy and Other Techniques. *J Am Chem Soc* **2014,** *136* (3), 978-985.
85. Mansuy, D.; Morgenstern-Badarau, I.; Lange, M.; Gans, P., An intermediate-spin iron(III) porphyrin complex with a vinylidene group inserted into a iron-nitrogen bond: paramagnetic susceptibility, EPR, and Moessbauer properties. *Inorg Chem* **1982,** *21* (4), 1427-1430.
86. Yatsunyk, L. A.; Walker, F. A., Structural, NMR, and EPR Studies of S = 1/2 and S = 3/2 Fe(III) Bis(4-Cyanopyridine) Complexes of Dodecasubstituted Porphyrins. *Inorg Chem* **2004,** *43* (2), 757-777.
87. Burstyn, J. N.; Roe, J. A.; Miksztal, A. R.; Shaevitz, B. A.; Lang, G.; Valentine, J. S., Magnetic and Spectroscopic Characterization of an Iron Porphyrin Peroxide Complex - Peroxoferrioctaethylporphyrin(1-). *J Am Chem Soc* **1988,** *110* (5), 1382-1388.
88. Palmer, G., Electron paramagnetic resonance of hemoproteins. In *Iron Porphyrins, Part II*, Lever, A. B. P.; Gray, H. B. E., Eds. Addison-Wesley: Reading, MA, 1983; pp 43–88.

89. Hagen, W. R., EPR spectroscopy as a probe of metal centres in biological systems. *Dalton T* **2006,** (37), 4415-4434.
90. Knowles, P. F.; Gibson, J. F.; Pick, F. M.; Bray, R. C., Electron-spin-resonance evidence for enzymic reduction of oxygen to a free radical, the superoxide ion. *Biochem J* **1969,** *111* (1), 53-8.
91. Dombrovskis, J. K.; Palmqvist, A. E. C., One-pot synthesis of transition metal ion-chelating ordered mesoporous carbon/carbon nanotube composites for active and durable fuel cell catalysts. *J Power Sources* **2017,** *357*, 87-96.
92. Chung, H.; Wu, G.; Higgins, D.; Zamani, P.; Chen, Z.; Zelenay, P., Heat-Treated Non-precious Metal Catalysts for Oxygen Reduction. In *Electrochemistry of N4 Macrocyclic Metal Complexes: Volume 1: Energy*, Zagal, J. H.; Bedioui, F., Eds. Springer International Publishing: Cham, 2016; pp 41-68.
93. Wang, Y.; Santiago-Aviles, J. J.; Furlan, R.; Ramos, I., Pyrolysis temperature and time dependence of electrical conductivity evolution for electrostatically generated carbon nanofibers. *Ieee T Nanotechnol* **2003,** *2* (1), 39-43.
94. Wiener, M.; Reichenauer, G.; Hemberger, F.; Ebert, H. P., Thermal conductivity of carbon aerogels as a function of pyrolysis temperature. *Int J Thermophys* **2006,** *27* (6), 1826-1843.